ELSEVIER

Ore Geology Reviews 28 (2006) 123–145

ORE GEOLOGY REVIEWS

www.elsevier.com/locate/oregeorev

Geology, geochemistry and mineralogy of indium resources at Mount Pleasant, New Brunswick, Canada ☆

W.D. Sinclair [a,*], G.J.A. Kooiman [b], D.A. Martin [c], I.M. Kjarsgaard [d]

[a] *Geological Survey of Canada, 601 Booth Street, Ottawa, Ontario, Canada K1A 0E8*
[b] *15 Kennedy Court, St. George, New Brunswick, Canada E0G 2Y0*
[c] *1858 Route 895, Elgin, New Brunswick, Canada E4Z 2N6*
[d] *15 Scotia Place, Ottawa, Ontario, Canada K1S 0W2*

Received 9 July 2001; accepted 27 March 2003
Available online 19 September 2005

Abstract

Indium-bearing deposits at Mount Pleasant, New Brunswick represent one of two major episodes of mineralization associated with granitic intrusions near the southwest margin of the Late Devonian Mount Pleasant caldera. Porphyry tungsten–molybdenum deposits, with negligible indium content, are associated with the earliest stage of intrusion and represent the first mineralization episode. Indium-bearing vein, replacement and breccia-hosted tin-base metal deposits are associated with a younger stage of intrusion and represent the second episode. The indium-bearing deposits are best developed in an eruptive center at Mount Pleasant referred to as the North Zone; indium resources in this area total 620 t In. The most significant individual deposit is the Upper Deep Tin Zone, which contains 476 t In in indicated and inferred resources totalling 1.7 Mt grading 280 g/t In, along with 0.68% Sn, 2.26% Zn and 0.29% Cu.

The indium-bearing tin-base metal deposits occur as sulfide-rich veins, breccias and replacement zones in both granitic rocks and associated volcanic and sedimentary rocks. Sphalerite, chalcopyrite, arsenopyrite and cassiterite are the most abundant ore minerals; a wide variety of other minerals occur in minor to trace amounts including löllingite, native bismuth, bismuthinite, wolframite, molybdenite, tennantite, stannite, kësterite, ferrokësterite, stannoidite, pyrite, galena, bornite, wittichenite and roquesite. Indium correlates most closely with high contents of zinc and copper, reflecting its concentration primarily in sphalerite and, to a lesser degree, in chalcopyrite. Electron-microprobe analyses for indium in sphalerite ranged mainly from <0.01% to 6.90% In; the highest values were encountered in sphalerite containing abundant inclusions of chalcopyrite. Indium appears to substitute for Zn and Fe according to the coupled substitution $CuIn \leftrightarrow 2(Zn,Fe)$, to form solid solution between sphalerite and roquesite. Indium content in chalcopyrite is much lower than in sphalerite; analyses ranged from 0.01% to 0.40% In.

Indium-rich sphalerite and associated minerals were deposited at temperatures that varied from 400 °C to less than 200 °C. Indium and associated metals were likely concentrated in magmatic–hydrothermal fluids derived from silicic magma now represented by a large body of granite that underlies Mount Pleasant and that degassed through small cupolas at the top of the magma chamber. Deposition of the metals occurred in response to cooling and dilution of the hot magmatic ore fluids, mainly as a result of mixing with meteoric fluids. This is similar to mechanisms proposed for other indium-bearing tin-polymetallic deposits.
© 2005 Elsevier B.V. All rights reserved.

Keywords: Indium; Tin; Base metals; Magmatic–hydrothermal; Mount Pleasant; New Brunswick

☆ Geological Survey of Canada Contribution Number 2002003.

* Corresponding author. Tel.: +1 613 992 9810; fax: +1 613 996 3726.
E-mail address: sinclair@nrcan.gc.ca (W.D. Sinclair).

0169-1368/$ - see front matter © 2005 Elsevier B.V. All rights reserved.
doi:10.1016/j.oregeorev.2003.03.001

1. Introduction

Indium is a relatively rare metal with increasing economic importance in a variety of high-tech applications including semiconductors, solar cells and display devices such as LCDs (liquid crystal displays) (Stevens and White, 1990; Schwartz-Schampera and Herzig, 1999a,b). It is also used to a large extent in low-temperature fusible alloys and solders. High demand for indium in late 1994 and 1995 outstripped supplies and the price of indium rose to US$551 per kg in December 1995 from US$131 per kg just twelve months previous (McCutcheon, 1996). Although the price of indium subsequently fell to previous levels, demand for indium continued to grow, particularly for LCDs and other electronic applications. In 2003 and 2004, uncertainties in market supply caused by a decrease in overall world production of indium caused prices to rise again, this time to historic highs. In early 2005, spot prices for indium were in excess of $1000 per kg.

The geology of indium and indium resources are poorly understood (Murao et al., 1991; Schwartz-Schampera and Herzig, 1999b). Although it is associated with zinc, copper and tin in a variety of ore deposits, indium is recovered primarily as a byproduct of zinc processing (Stevens and White, 1990) and most known resources are related to zinc-rich deposits (Roskill, 1996). However, substantial amounts of indium are recovered from copper ores of the Kidd Creek deposit in Canada and the Neves Corvo deposit in Portugal (Hannington et al., 1999; Schwartz-Schampera and Herzig, 1999a). Indium has also been recovered from the processing of lead and tin ores (Halsall, 1988).

Base-metal deposits containing tin were discovered and explored at Mount Pleasant in the 1950s and 1960s, during which time indium-bearing minerals were initially identified (Boorman and Abbott, 1967; Sutherland and Boorman, 1969). By the late 1960s, exploration had shifted to large, low-grade, porphyry-type tungsten–molybdenum deposits, one of which was mined from 1983 to 1985 (Kooiman et al., 1986). In the latter part of the 1980s and early 1990s, detailed surface and underground exploration again focused on the smaller, but higher-grade tin-bearing base metal deposits. Stimulated by the potential value of indium as a co-product in these deposits, particularly in view of the dramatic rise in the price of indium in the mid-1990s, an assessment of the indium resources at Mount Pleasant was undertaken by Piskahegan Resources Ltd. and Adex Mining Corporation from 1994 to 1997. Part of this assessment included a joint project between Piskahegan and the Geological Survey of Canada to determine the mineralogical distribution of indium, primarily by electron-microprobe analysis of indium-bearing minerals. This work has shown that, despite the presence of indium minerals such as roquesite, and high levels of indium in chalcopyrite and stannite group minerals, the bulk of the indium resources reside in sphalerite. The results of this work also provide insights regarding the genesis of the indium-rich deposits at Mount Pleasant and are the basis for this paper.

2. Geological setting of the Mount Pleasant deposits

The Mount Pleasant deposits are situated in southern New Brunswick within the Appalachian Orogen in eastern Canada. They occur within Late Devonian Piskahegan Group volcanic and sedimentary rocks that are the remnants of a large epicontinental caldera complex (McCutcheon et al., 1997). The caldera rocks are undeformed and were emplaced in an anorogenic or post-collisional, pre- to syn-extensional setting following the Acadian Orogeny. The caldera is bounded to the east and west by polydeformed Ordovician and Silurian turbiditic metasedimentary rocks and to the south by dioritic to granitic rocks of the Saint George Batholith that range from Late Silurian to Devonian in age (Fig. 1). To the north, the caldera is disconformably overlain and concealed by Carboniferous sedimentary rocks. Mount Pleasant is located near the southwest margin of the caldera complex.

Piskahegan Group rocks at Mount Pleasant include several layers of rhyolitic ash flow tuffs formally called Little Mount Pleasant Tuff (McCutcheon et al., 1997) and informally referred to as quartz–feldspar porphyry (Figs. 2 and 3). The ash flow tuff layers are separated by discontinuous units of sedimentary breccia that are as much as 100 m thick near the margin of the caldera and pinch out within 1000 m. These breccia units, which are part of the Scoullar Mountain Formation (McCutcheon et al., 1997), consist mainly of angular to subrounded clasts of fine-grained metasedimentary rocks derived from the metasedimentary rocks that form the western boundary of the caldera. Along the caldera margin, where clast size is greatest, these sedimentary breccia units probably represent talus breccias. Overlying the ash flow tuffs is a rhyodacitic flow of feldspar porphyry. This unit is likely an extrusive equivalent of the McDougall Brook Porphyritic Microgranite, which forms a large intrusive body northeast of Mount Pleasant (McCutcheon et al., 1997).

The Piskahegan Group rocks at Mount Pleasant have been intruded by small subvolcanic plutons or cupolas

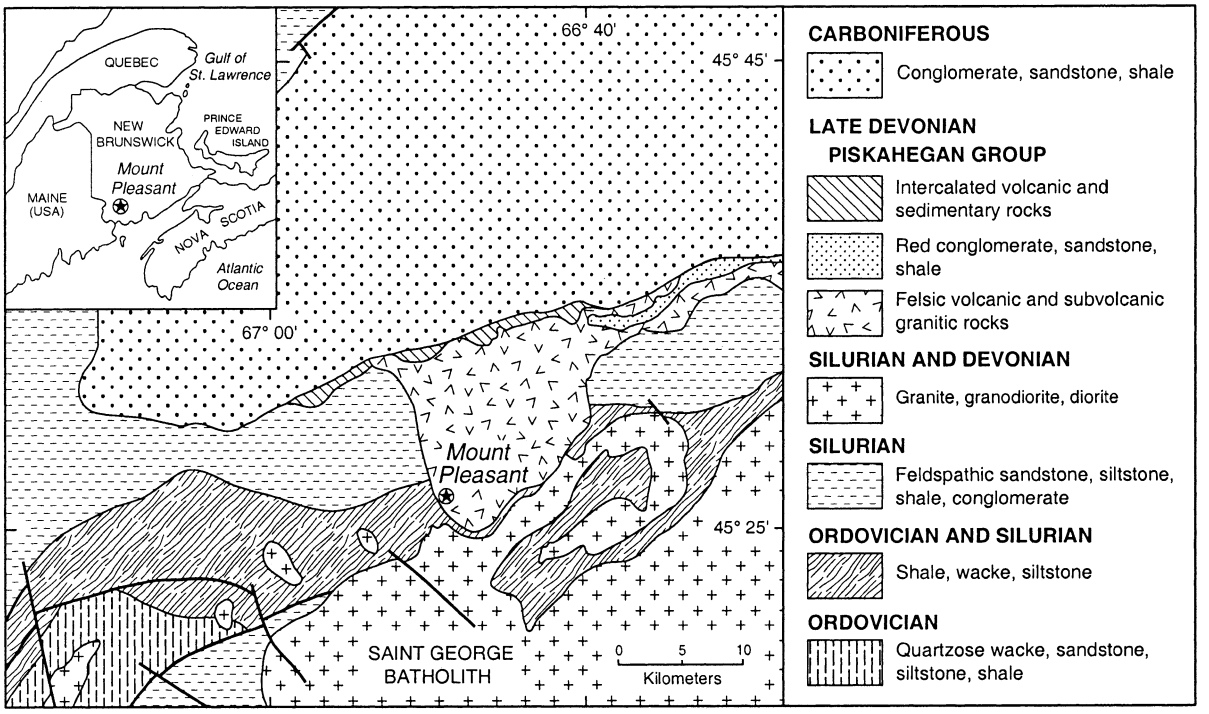

Fig. 1. Regional geological setting and location of Mount Pleasant (modified from McLeod et al., 1994).

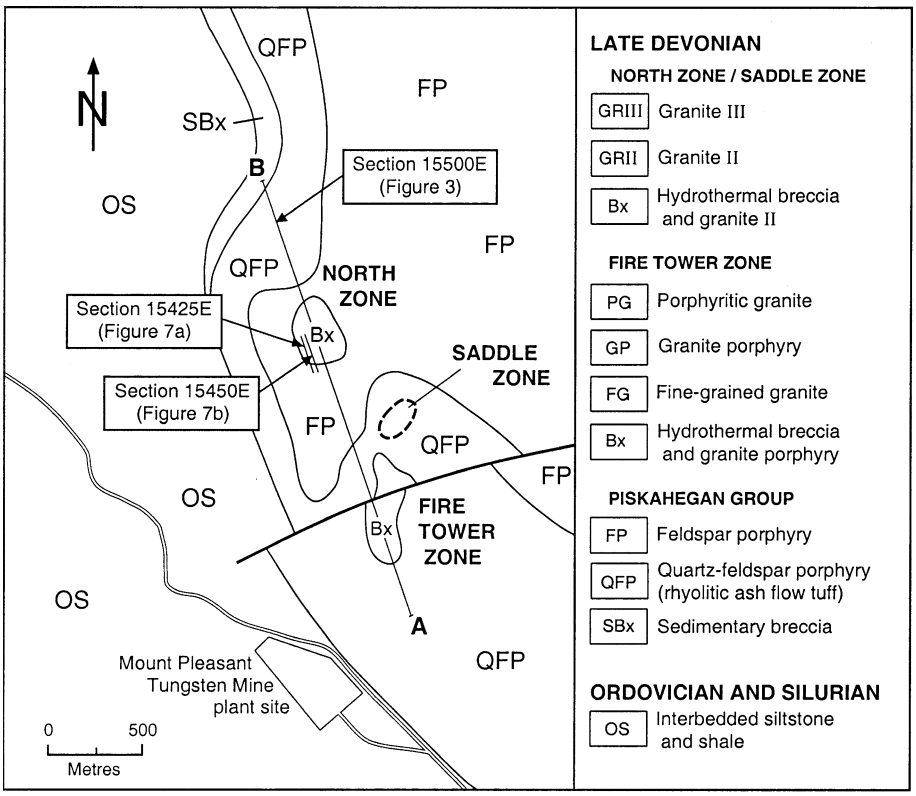

Fig. 2. Geological map of Mount Pleasant showing the location of the North Zone, Fire Tower Zone and Saddle Zone. Line AB is the location of cross-section 15500E shown on Fig. 3. Locations of cross-sections 15425E and 15450E shown on Fig. 7 are also indicated.

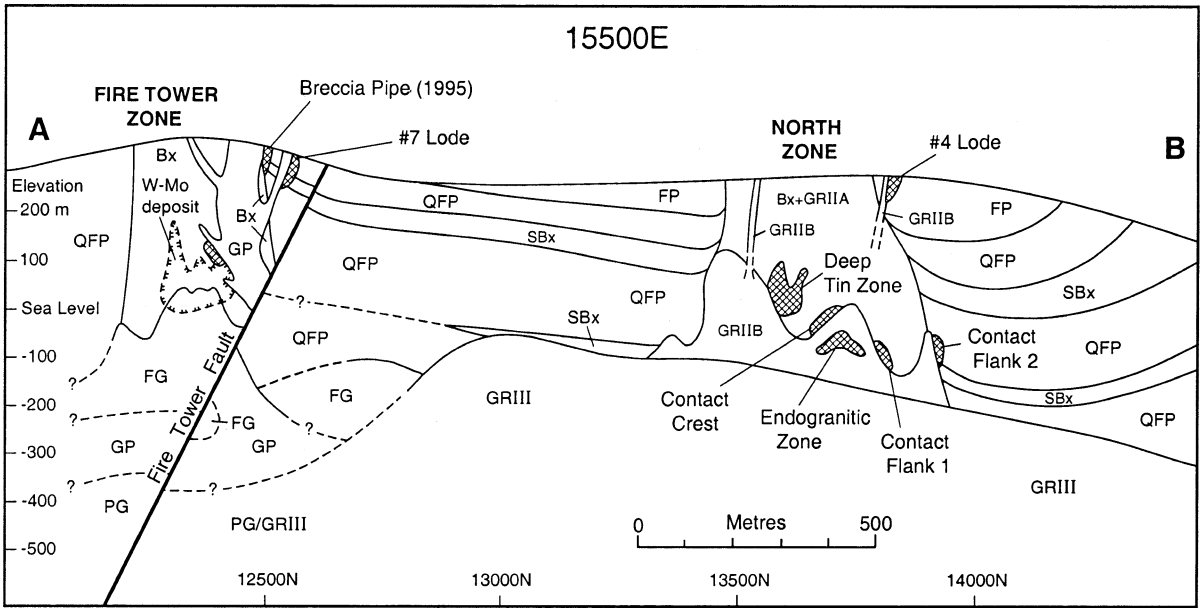

Fig. 3. Cross-section 15500E through the Fire Tower Zone and the North Zone. Location of section and legend as shown on Fig. 2.

of granitic rocks collectively named Mount Pleasant Porphyry (McCutcheon et al., 1997). Detailed studies of underground exposures and drill core at Mount Pleasant have documented at least three different stages of granitic intrusion that are generally similar mineralogically and chemically. Texturally, they range from aplitic to porphyritic and, in the youngest stages, to medium-grained equigranular. Fluorite is a common accessory mineral, topaz is present in places. Chemically, they are high-silica (74% to 77% SiO_2), fluorine-rich (0.3% to 1% F) granites with elevated contents of Li (50 to 600 ppm) and Rb (700 to 1200 ppm) in particular (Kooiman et al., 1986; Sinclair, 1994). The chemical data and the presence of primary topaz suggest that the Mount Pleasant granites are compositionally analogous to topaz granites (cf. Pichavant and Manning, 1984). A Late Devonian age of emplacement of the Mount Pleasant granites is indicated by a K–Ar age of 361 ± 9 Ma from biotite hornfels at the contact with the youngest stage of granite (GSC89-113 in Hunt and Roddick, 1990).

Two separate areas at Mount Pleasant where Piskahegan Group rocks have been brecciated and intruded by granitic rocks have been designated the North Zone and the Fire Tower Zone (Fig. 2). The North Zone contains the most important indium-bearing tin-base metal resources outlined to date along with some poorly defined tungsten–molybdenum zones. The Fire Tower Zone hosts mainly tungsten–molybdenum deposits and some small indium-bearing tin-base metal zones. A third area, referred to as the Saddle Zone, contains mineralized zones with tin and base metals that have been intersected in exploratory diamond drill holes. No detailed assessment has been made of the mineral resources in this area, including its potential for indium.

3. Geology and indium resources of the Fire Tower Zone

The geology of the Fire Tower Zone has been described previously by Parrish and Tully (1978) and Kooiman et al. (1986). The main host rocks in the Fire Tower Zone consist of a complex suite of magmatic–hydrothermal breccias that crosscut volcanic and sedimentary rocks (Fig. 3). The breccias form a roughly oval-shaped vertical pipe that is about 225 by 450 m at surface. The breccias consist of multiple phases that range from clast-supported breccias with angular fragments to matrix-supported breccias with rounded fragments. The fragments are mainly of volcanic rocks, although in many places the textures and lithologies of the fragments have been obscured by hydrothermal alteration. The breccia pipe is underlain by fine-grained granite that represents the oldest granitic intrusive stage in the Fire Tower Zone. In places, the lowermost parts of the breccia pipe are characterized by zones of predominantly granitic fragments that appear to have been derived from underlying brecciated fine-grained granite. Both the breccias and the fine-grained granite are crosscut by a younger stage of granite porphyry with a

fine-grained to aphanitic groundmass. A coarser-grained, porphyritic granite underlies the Fire Tower Zone at depth and represents the youngest stage of intrusion.

3.1. Tungsten–molybdenum deposits in the Fire Tower Zone

Tungsten–molybdenum deposits in the Fire Tower Zone occur mainly in the lower part of the breccia pipe and the upper part of the underlying fine-grained granite, and to a lesser extent in associated volcanic rocks. They are large, low-grade porphyry-type deposits characterized by extensive stockworks of mineralized fractures and quartz veinlets (Fig. 4), and disseminated ore minerals in breccia matrix. Higher grade zones in areas of intense fracturing are 200 to 300 m across and as much as 100 m in vertical extent; they are surrounded by lower-grade zones characterized by more widely spaced fractures that extend for hundreds of metres into surrounding rocks. Wolframite and molybdenite, along with minor amounts of native bismuth and bismuthinite, are the principal ore minerals and are typically fine-grained. Arsenopyrite, löllingite, quartz, topaz and fluorite are the most abundant gangue minerals.

Alteration associated with the tungsten–molybdenum deposits includes intense and pervasive greisen-type alteration consisting of quartz+topaz+fluorite, which is associated with higher-grade mineralized zones. Surrounding lower-grade zones are characterized by an assemblage of quartz+biotite+chlorite+fluorite on fracture and vein selvages. Propylitic alteration (chlorite+sericite) extends for hundreds of metres beyond the mineralized zones.

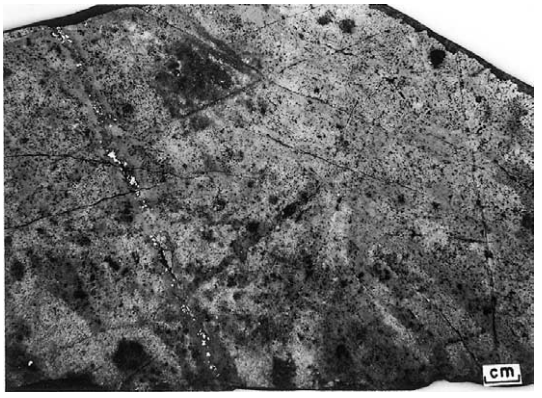

Fig. 4. Altered breccia cut by stockwork of mineralized fractures and quartz veinlets; white grains in photograph are wolframite (reflected light). Fire Tower Zone tungsten–molybdenum porphyry deposit. GSC 2000-180M.

Formation of the tungsten–molybdenum deposits appears to be related to the emplacement of fine-grained granite. Crosscutting relationships between mineralized fractures and veinlets indicate that mineralization occurred in multiple stages, the earlier of which were more tungsten- and bismuth-rich and the later more molybdenum-rich. Sparse molybdenite-bearing fractures in fine-grained granite below the main mineralized zone appear to represent the final stage of mineralization associated with crystallization of this granite. The tungsten–molybdenum deposits clearly predate crosscutting dikes of unmineralized granite porphyry that truncate mineralized stockwork zones.

Tungsten–molybdenum resources in the Fire Tower Zone prior to mining were 22 Mt grading 0.21% W, 0.10% Mo and 0.08% Bi (Parrish and Tully, 1978). A higher-grade deposit within this resource that was outlined for production contained 9.4 Mt grading 0.31% W and 0.12% Mo (Kooiman et al., 1986). The indium content of the tungsten–molybdenum deposits is relatively low, on the order of 1 ppm In or less, based on analysis of nearly 100 samples of typical ore material. Contamination by later stages of indium-bearing mineralization may account for some of the higher values (up to 15 ppm In) encountered in a few of these samples.

3.2. Tin-base metal-indium deposits in the Fire Tower Zone

Indium-bearing tin-base metal deposits occur as irregular veins and mineralized breccias that are distributed irregularly throughout the Fire Tower Zone and surrounding rocks. They are typically associated with dikes of granite porphyry that are themselves altered and mineralized. In many places, both the dikes of granite porphyry and the associated tin-base metal deposits truncate or crosscut tungsten–molybdenum stockworks. Individual veins typically range from 1 cm to 2 m wide and up to several metres in strike length although a few large veins are up to 10 m wide and 100 m long. The larger veins generally have irregular but sharp wall-rock boundaries that pinch and swell. The veins consist mainly of chlorite, with abundant fluorite, and a highly varied assemblage of disseminated to massive sulfides (Fig. 5a). Mineralized breccias (Fig. 5b) are irregular bodies that are associated in many places with larger veins, as in the #7 lode where they form a zone 18 m wide associated with two large veins (Petruk, 1973). They also occur as small vertical pipes, an example of which was discovered at surface in the Fire Tower Zone in 1995. This pipe is

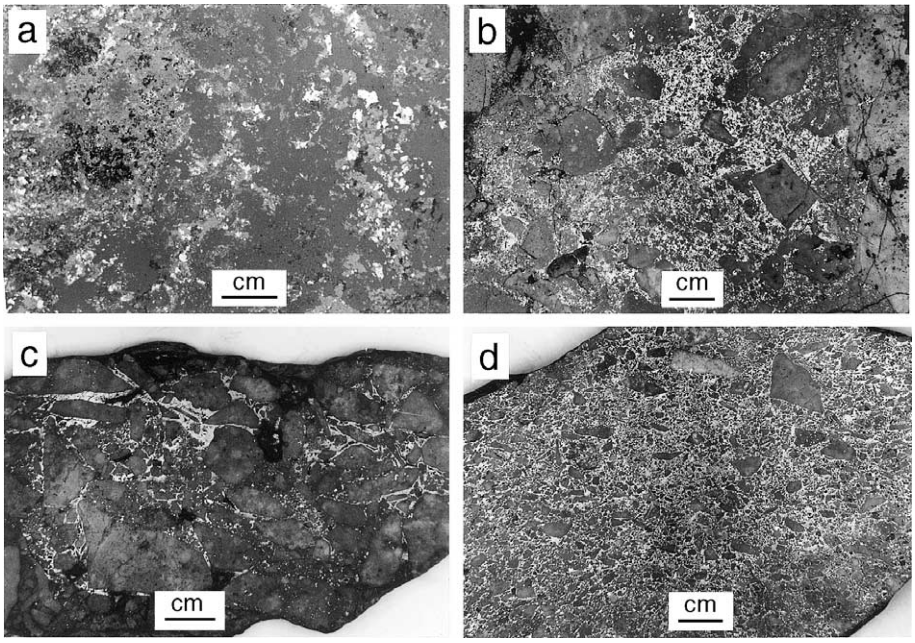

Fig. 5. Examples of indium–tin-base metal-bearing veins and breccias from the Fire Tower Zone. (a) Massive chlorite (dark grey) and fluorite (black) with disseminated to massive sulfides, mainly sphalerite (light grey) and galena (white); Fire Tower North deposit. GSC 2000-180E. (b) Heavily disseminated sulfides (white), mainly sphalerite and chalcopyrite, in matrix of felsic breccia; #7 Lode deposit. GSC 2000-180G. (c) Felsic breccia consisting of clast-supported fragments with sphalerite (white) and cassiterite in matrix; Breccia Pipe 1995 deposit. GSC 2000-180H. (d) Felsic breccia consisting of matrix-supported fragments with abundant sulfides (white) in matrix; Breccia Pipe 1995 deposit. GSC 2000-180I.

roughly circular, with a diameter of 10 m and a vertical extent of at least 100 m. Breccia fragments are angular and range from less than 1 cm to several centimetres in size. In some places, the fragments are tightly packed, with spaces between the fragments infilled to a large extent by fine-grained sulfides and cassiterite (Fig. 5c). In other places, breccia fragments are separated and supported by the breccia matrix which consists of chlorite, fluorite and heavily disseminated to massive sulfides (Fig. 5d).

The indium-bearing tin-base metal veins and breccias contain a highly varied assemblage of sulfide and oxide minerals, various aspects of which have been documented by Boorman and Abbott (1967), Sutherland and

Table 1
Estimated resources of indium and other elements in tin-base metal deposits at Mount Pleasant

	Tonnes ($\times 10^6$)	In (g/t)	Sn (%)	Zn (%)	Cu (%)	Bi (%)	WO_3 (%)	MoS_2 (%)
Fire Tower Zone:								
#7 Lode (indicated resource)	0.014	102	0.54	5.55	0.70		0.07	
Fire Tower North (West Body) (indicated resource)	0.25	206	0.19	2.24	0.14		0.28	
Breccia Pipe (1995) (estimated resource)	0.02	300	1.50	5.40	1.80			
North Zone:								
Upper Deep Tin Zone (indicated resource)	1.2	275	0.76	2.08	0.35	0.11	0.07	0.05
Upper Deep Tin Zone (inferred resource)	0.5	291	0.50	2.68	0.16			
Endogranitic Zone (indicated resource)	1.4	45	0.88	0.20	0.09		0.07	
Contact Flank (indicated and inferred resource)	0.9	45	1.00	0.54	0.19		0.27	
Contact Crest (indicated resource)	0.7	45	0.89	0.36	0.17		0.12	
#4 Lode (indicated and inferred resource)	0.1	91	0.24	0.96	0.08		0.01	
Indium resource — Upper Deep Tin Zone:		476 t In (based on 60 g/t In cut-off grade)						
Indium resource — North Zone:		620 t In (based on 60 g/t In cut-off grade for Upper Deep Tin Zone and #4 lode, and 0.2% Sn cut-off grade for other deposits)						

Boorman (1969), Petruk (1964, 1973), Kissin (1989), and Kissin and Owens (1989). Sulfides range in size from minute disseminated grains to irregular masses several cm across. They consist mainly of sphalerite, chalcopyrite, galena and arsenopyrite, along with minor amounts of pyrite, löllingite, molybdenite, tennantite, native bismuth, and bismuthinite. Sulfides present in trace amounts include stannite, kësterite, stannoidite, aikinite and cosalite; the copper–indium mineral roquesite is rare. Cassiterite and wolframite are the principal oxide minerals and occur mainly as minute disseminated grains, although wolframite in places forms crystal aggregates several centimetres long.

Indium resources in the Fire Tower Zone are concentrated in the tin-base metal veins and breccia zones. Deposits for which indium resources have been identified are listed in Table 1. The content of indium in these deposits ranges from 100 to 300 g/t on average, although indium distribution is highly varied and individual assays range from a few grams per tonne to nearly 4000 g/t. All of the identified tin-base metal deposits in the Fire Tower Zone are relatively small and the indium resources of this area appear to be limited.

4. Geology and indium resources of the North Zone

The geology of the North Zone, previously described by Ruitenberg (1963, 1967), Sinclair et al. (1988), and Inverno (1991), has been refined as a result of recent exploration programs. In many respects, the geology of the North Zone is comparable to that of the Fire Tower Zone in that it is the site of an eruptive centre characterized by complex breccias and subvolcanic intrusive rocks that occupy an oval-shaped vertical pipe about 250 by 300 m across (Figs. 2 and 3). The breccias are composed mainly of fragments of quartz–feldspar porphyry, feldspar porphyry and granitic rocks, although in many places intense hydrothermal alteration has obscured both the identities of the fragments and the textural relationships among them. A younger suite of breccias that form dike- or pipe-like bodies crosscut the older breccias and surrounding rocks. The breccias are also intruded and underlain at depth by several intrusive stages of granite, the three main phases of which have been designated I, II, and III. These granites are similar mineralogically and chemically to the three phases in the Fire Tower Zone: fine-grained granite, granite porphyry and porphyritic granite, respectively.

The distribution of granite I, the oldest of the intrusive phases in the North Zone, is poorly known. Altered and brecciated granite I locally hosts low-grade tungsten–molybdenum zones but in many places it has been displaced by younger intrusions. Like the fine-grained granite in the Fire Tower Zone, the emplacement of granite I appears to be closely related to the initial development of the breccia pipe and the formation of low-grade tungsten–molybdenum zones.

Granite II has intruded and displaced much of the North Zone breccia complex although its relationship to the breccias is in many places obscured by alteration. Granite II is similar mineralogically to granite I, but the groundmass is typically finer-grained and quartz and feldspar phenocrysts are more prominent. Much of granite II is pervasively sericitized and chloritized. It is also characterized locally by fluid saturation textures such as miarolitic cavities and comb quartz layers (Sinclair et al., 1988). The latter occur in places along the margins and in the upper parts of small intrusions or cupolas. They consist of parallel to subparallel layers of quartz that generally range from less than 1 mm to several centimetres or more in thickness and are separated by interlayers of fine-grained, aplitic granite (Fig. 6a). Prismatic quartz crystals in the layers are oriented roughly perpendicular to the planes of layering (Fig. 6b) and appear to have grown on a crystallized aplitic substrate inward toward the center of the intrusion. Comb quartz layers represent one type of unidirectional solidification texture (UST) that occurs in high-level felsic intrusions associated with certain types of porphyry and other intrusion-related deposits (Shannon et al., 1982; Kirkham and Sinclair, 1988). They are significant because individual layers likely crystallized from pockets of exsolved magmatic–hydrothermal fluid and the development of multiple layers reflects a continuous supply of magmatic fluid from subjacent magma (Lowenstern and Sinclair, 1996).

Two separate phases of granite II have been recognized on the basis of contact relationships; the older of these is referred to as granite IIA and the younger as granite IIB (Fig. 3). Granite IIA appears to occupy much of the upper part of the breccia pipe where its distribution is poorly defined. Granite IIB occupies a number of well-defined protrusions or cupolas in the lower part of the pipe (Fig. 3). The upper contact of granite IIB is distinguished in many places by the development of comb quartz layers. Fine-grained to aphanitic, locally banded dikes that appear to be related to granite IIB have intruded the overlying breccias and associated host rocks. Indium-bearing tin-base metal zones in the North Zone are associated primarily with granite IIB.

At depth in the North Zone, granite IIB has been intruded and truncated by granite III. The upper surface

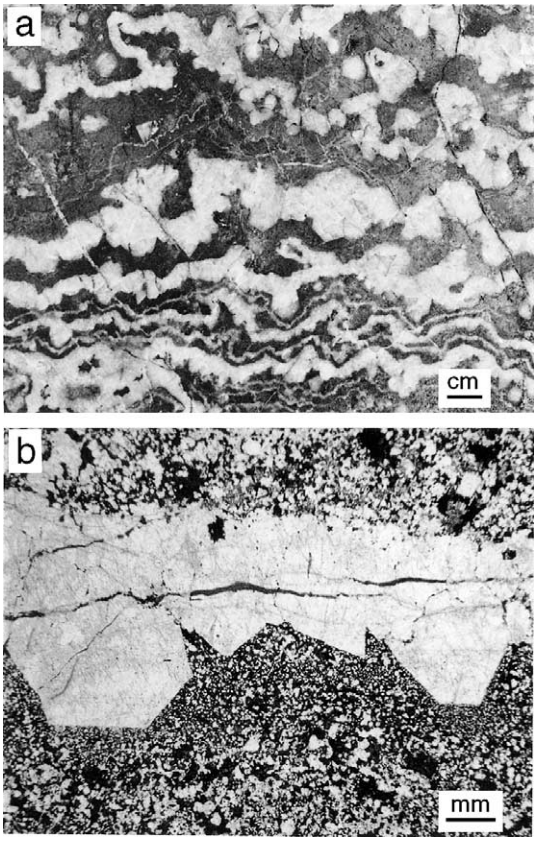

Fig. 6. (a) Layers of comb-textured quartz separated by interlayers of chloritized aplitic granite II; growth direction of the layers was towards the bottom of the photograph. GSC 204152-H. (b) Photomicrograph of a thin comb quartz layer in Granite II showing euhedral termination of quartz crystals approximately perpendicular to the layer; the very fine grained texture of the granite adjacent to the crystal faces likely resulted from pressure quenching related to sudden expansion and escape of exsolved magmatic fluid in which the crystals were growing. GSC 204152-T.

of granite III is subhorizontal and has relatively sharp contacts characterized by chilled margins and, in places, by narrow, 1 to 2 cm wide layers of unidirectional feldspar crystals, another type of UST. Granite III extends to the south and is likely continuous with porphyritic granite that underlies the Fire Tower Zone (Fig. 3). No significant mineral resources have been found within or directly associated with granite III.

4.1. Tungsten–molybdenum deposits in the North Zone

Tungsten and molybdenum deposits in the North Zone are similar to those in the Fire Tower Zone, but smaller. They occur as discontinuous bodies that form a ring-shaped zone hosted mainly within the North Zone breccias and to a lesser extent in underlying brecciated granite I (Parrish and Tully, 1978). Mineral resources in the tungsten–molybdenum deposits of the North Zone have been estimated at about 11.5 Mt grading 0.20% W, 0.06% Mo, 0.09% Bi and 0.10% Sn (Parrish and Tully, 1978). The tin content of these deposits probably reflects the superposition of tin-base metal mineralization on the tungsten–molybdenum deposits. Indium content of the tungsten–molybdenum deposits, where they have not been overprinted by tin-base metal mineralization, is similar to that of the Fire Tower Zone tungsten–molybdenum deposits, i.e., typically 1 ppm In or less.

4.2. Tin-base metal-indium deposits in the North Zone

Tin-base metal deposits, many of which contain significant amounts of indium, are best developed in the North Zone at Mount Pleasant. Indium resources currently identified in these deposits total 620 t In (Table 1), which ranks Mount Pleasant as one of the most significant unexploited deposits of indium in the world.

Indium-bearing tin-base metal deposits in the North Zone occur over a vertical range of nearly 400 m and have characteristics that differ according to their level of emplacement. Numerous small sulfide-rich veins, breccias and replacement zones, which occur near surface, were originally explored for tin in the 1960s (Hosking, 1963; Ruitenberg, 1963, 1967; Petruk, 1964). The mineralized veins and breccia zones are associated with aphanitic, locally banded dikes of granite II that are commonly brecciated, altered and mineralized in the vicinity of the deposits. The mineralogy of the deposits consists principally of fine to very fine grained cassiterite, arsenopyrite, löllingite, sphalerite and chalcopyrite, with lesser amounts of stannite, pyrite, marcasite, galena, wolframite, molybdenite, tennantite, chalcocite, bornite, native bismuth, bismuthinite and wittichenite. Other associated minerals include abundant fluorite and chlorite. In the immediate vicinity of the deposits, the host rocks are typically altered to a fine-grained, greisen-type assemblage of quartz, sericite, topaz and fluorite. The near-surface deposits, however, contain limited resources of indium; the #4 Lode, one of the largest of these deposits, contains approximately 9 t of indium in 100,000 t of mineralized material averaging 91 g/t In (Table 1).

Larger indium-bearing tin-base metal deposits occur at depths of 200 to 400 m below surface in the North Zone. They include the Deep Tin Zone, Contact Crest, Contact Flank and Endogranitic Zone deposits (Fig. 3). The Deep Tin Zone deposit was discovered in the early

1970s when drilling was focused primarily on porphyry tungsten–molybdenum zones. Although tin-bearing zones were subsequently discovered at lower levels in the mid-1980s, the name Deep Tin Zone was retained. The results of the most recent exploration, in the mid-1990s, have shown that this deposit consists of two distinct parts, which have been designated the Upper Deep Tin Zone and the Lower Deep Tin Zone (Fig. 7a, b). The Upper Deep Tin Zone consists of steeply dipping to nearly horizontal mineralized zones that are adjacent to a cupola of granite IIB in the southern part of the North Zone and extend in a northerly direction outward into granite IIA and associated breccia. In the vicinity of the mineralized zones, granite IIB contains comb quartz layers developed in a zone as much as 25 m wide at the contact (Fig. 7a). The host rocks are highly silicified and brecciated; ore minerals occur in veins and veinlets, as breccia matrix and vug fillings, and as disseminated grains and clusters of grains replacing altered host rocks. Styles of mineralization are similar to those in other deposits in the North Zone, examples of which are shown in Fig. 8. Sphalerite, chalcopyrite, arsenopyrite and cassiterite are the most abundant ore minerals; other minerals that occur in minor to trace amounts include löllingite, tennantite, stannite, stannoidite, wittichenite and roquesite.

The Upper Deep Tin Zone deposit contains 476 t In, the largest individual resource of indium outlined to date at Mount Pleasant (Table 1). Indicated and inferred resources, based on a cut-off grade of 60 g/t In, total 1.7 Mt grading 280 g/t In, 0.68% Sn, 2.26% Zn and 0.29% Cu. With additional exploration, the indium resource in this zone is likely to increase in size. The current resource estimates are based on exploration conducted primarily along the northern margin of the southern cupola; however, isolated drill intersections suggest that the Upper Deep Tin Zone extends to the west and south of the cupola.

The Lower Deep Tin Zone lies below and outward from the Upper Deep Tin Zone (Fig. 7). It consists primarily of cassiterite and arsenopyrite veinlets and stockworks with a relatively low sulfide content overall. Indium content of the Lower Deep Tin Zone is relatively low; assay values typically range from 5 to 20 g/t In and are considered too low to include this zone as a potential indium resource.

The Contact Crest and Contact Flank deposits occur below the Deep Tin Zone along the upper contact and sides of granite IIB (Fig. 3). The host rocks for these deposits are mainly granite IIA and breccia, and to a lesser extent volcanic and sedimentary rocks. These deposits are similar to the Upper Deep Tin Zone with

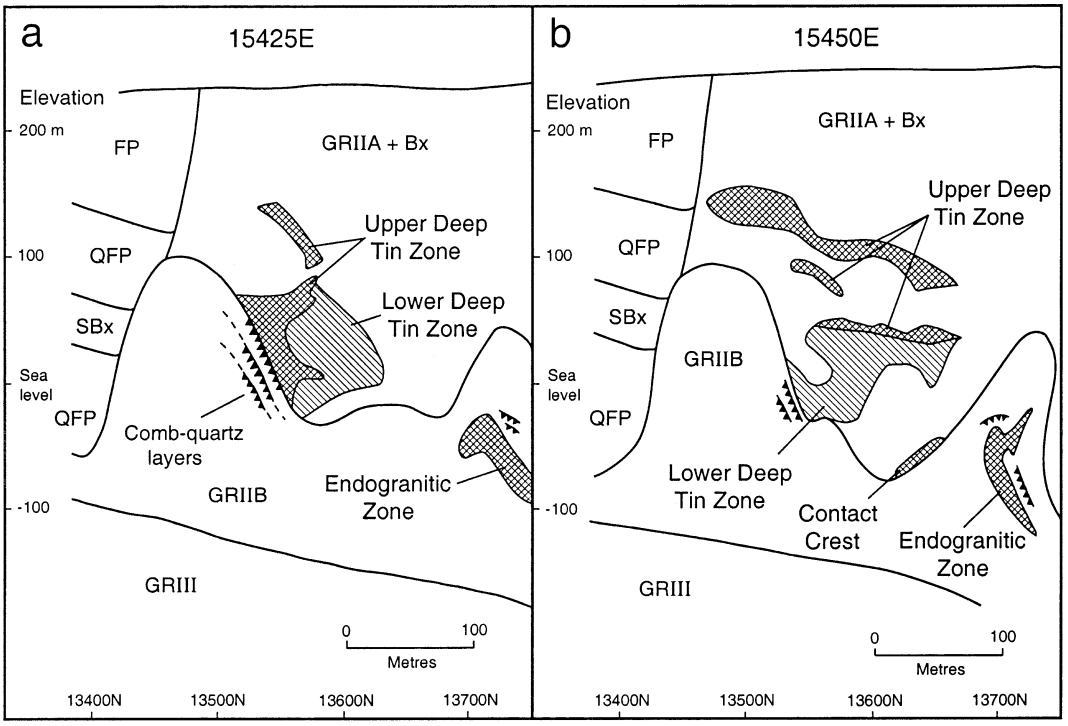

Fig. 7. Cross-sections through the North Zone showing indium-bearing tin-base metal deposits. Location of sections and legend as shown on Fig. 2. (a) Section 15425E. (b) Section 15450E.

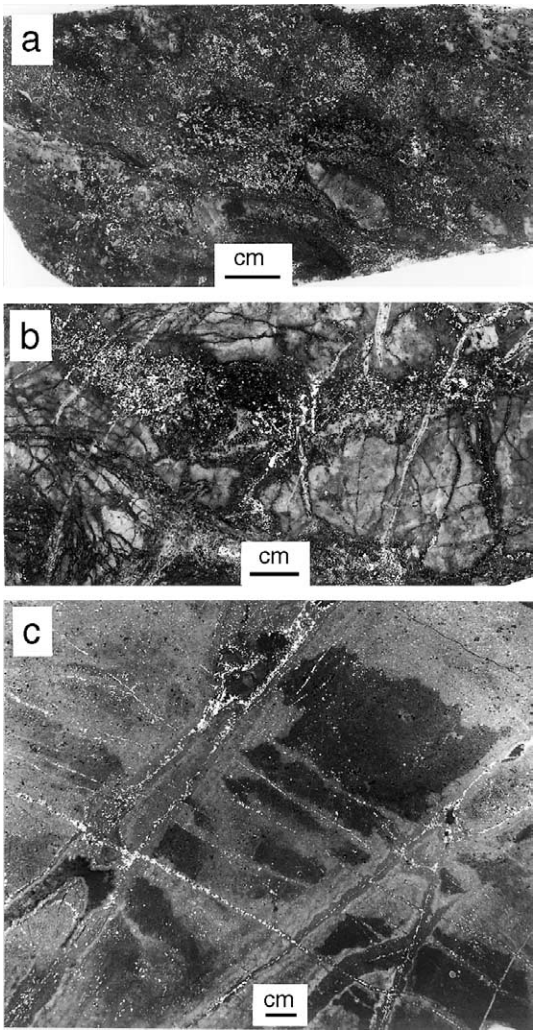

Fig. 8. Examples of indium–tin-base metal-bearing veins and breccias from the North Zone. (a) Fine-grained disseminated sulphides (white), mainly chalcopyrite, in felsic breccia; Contact Crest deposit. GSC 2000-180A. (b) Brecciated and silicified granite with cassiterite and sulfides (white) in fractures and heavily disseminated locally in the breccia matrix; Endogranitic Zone deposit. GSC 2000-180D. (c) Chloritized granite IIB (black) overprinted by fracture-controlled arsenopyrite (white), cassiterite and fluorite and associated quartz–topaz alteration (light grey); Endogranitic Zone deposit. GSC 2000-180K.

respect to the principal ore minerals and their modes of occurrence, particularly as disseminated grains in breccia matrix (Fig. 8a). The indium content of these deposits averages 45 g/t In (Table 1).

The Endogranitic Zone is the deepest and the largest of the tin-base metal-indium deposits in the North Zone. It is an irregular, subhorizontal to steeply dipping, roughly tabular deposit that occurs almost entirely within granite IIB (Figs. 3 and 7), except in a few places where it crosscuts the granite IIA/granite IIB contact. It also extends locally into adjacent volcanic and sedimentary rocks. At least five successive stages of alteration and related mineralization in the Endogranitic Zone have been recognized by Inverno (1991) and ourselves. The first stage of alteration consists of pervasive sericitic alteration of the host granitic rocks; this alteration is crosscut by weak, fracture-controlled to pervasive chloritic alteration that constitutes the second stage. The third and fourth stages consist primarily of quartz–topaz and chlorite–biotite alteration, respectively. The fifth stage is characterized by clay alteration, consisting mainly of kaolinite.

Only the third and fourth stages of alteration are associated with significant tin and base metal mineralization. The third alteration stage, characterized by a greisen-type assemblage of fine-grained quartz and topaz, has replaced previously sericitized and chloritized granite along fracture and veinlet selvages. The alteration envelopes are up to several centimetres wide and in places extend continuously between closely spaced fractures. Cassiterite, arsenopyrite, and fluorite, along with minor amounts of sphalerite, stannite, chalcopyrite, bismuthinite, chalocite, pyrite, covellite and roquesite occur in veinlets, along hairline fractures and as disseminated grains in the altered wall rocks (Fig. 8b, c). The fourth alteration–mineralization stage in the Endogranitic Zone is represented by dark to pale green rock that is composed mainly of dense, fine-grained Fe-rich chlorite and/or biotite. This alteration forms massive patches or lenses up to 4 m wide that are superimposed on or crosscut earlier stages of alteration, including the greisen-type quartz–topaz alteration. Occurring within the dense chlorite–biotite rock are local clusters of topaz, patches of coarse fluorite and irregular zones of weakly to heavily disseminated, fine-grained cassiterite. Other minerals present in minor amounts as disseminated grains or in small clusters include arsenopyrite, löllingite, sphalerite, chalcopyrite, galena, native bismuth, bismuthinite, wolframite, molybdenite, pyrite and magnetite. The Endogranitic Zone is primarily a tin deposit with a resource of 1.4 Mt grading 0.88% Sn, based on a cut-off grade of 0.2% Sn (Table 1). The indium content of the deposit averages 45 g/t In, similar to the indium content of the Contact Crest and Contact Flank deposits.

5. Indium geochemistry of the deposits

Distribution of indium in the tungsten–molybdenum and tin-base metal deposits was studied by analyzing the indium content of 353 samples from the deposits. Determination of indium was based on total dissolution of samples by multiacid attack (nitric, perchloric and

hydrofluoric acids) followed by lithium metaborate fusion of any residual material. Analysis was done by inductively coupled plasma mass spectroscopy at XRAL Laboratories Ltd. (Don Mills, Ontario). Reliability of the measurements, checked by CANMET certified reference ore sample MP-1a, is within 5% error. Data for the other elements (Sn, W, Mo, Bi, Cu, Pb, Zn) are from assay records of Brunswick Tin Mines Ltd., Mount Pleasant Tungsten Mine and Lac-Billiton Tin Project.

The contents of indium and other major and minor elements in the Mount Pleasant deposits are shown as inter-element plots in Fig. 9 and a correlation matrix for

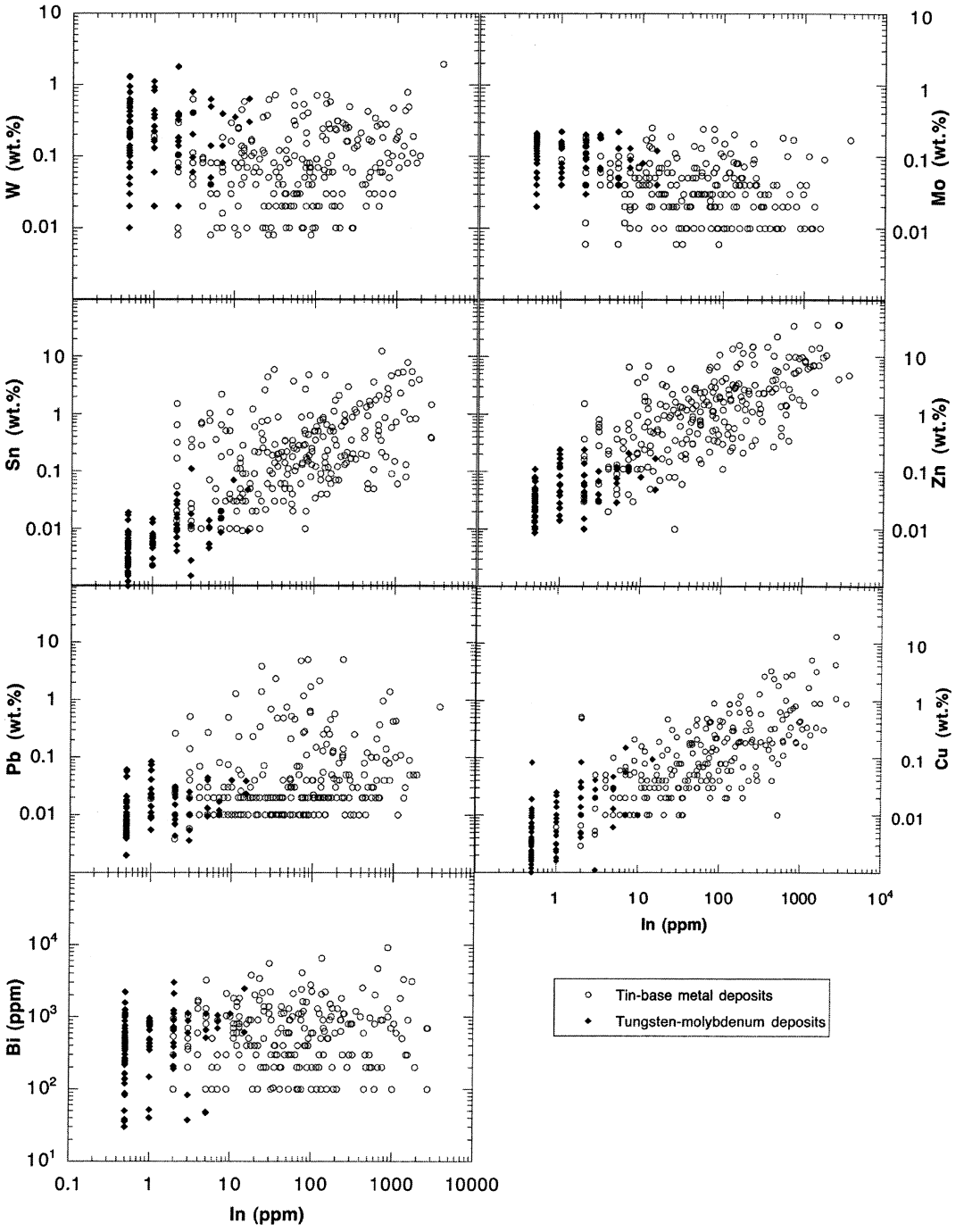

Fig. 9. Interelement plots for major and minor elements in tungsten–molybdenum and tin-base metal-indium deposits at Mount Pleasant ($n = 353$).

these elements is given in Table 2. Major and minor element associations reflect the two different mineralogical assemblages in the Mount Pleasant deposits: a low-sulfide assemblage represented by the tungsten–molybdenum–bismuth deposits and a high-sulfide assemblage that characterizes the tin-base metal deposits. Indium in the low sulfide assemblage, based on analysis of 97 tungsten–molybdenum ore samples, has a median value of <1 ppm In, although values range from <1 to 15 ppm In. The low values reflect the low content of indium in the principal ore minerals such as wolframite and molybdenite, and in associated sulfide minerals such as arsenopyrite, löllingite and bismuthinite. The higher values appear to correlate with small, but anomalous amounts of Cu, Zn and Sn, which are likely related to weak overprinting of the tungsten–molybdenum ores by the tin-base metal stage of mineralization. Median values for Cu, Zn and Sn in these samples are 52, 340 and 51 ppm, respectively, although values range as high as 1500 ppm Cu, 2400 ppm Zn and 1100 ppm Sn.

Indium, along with tin, zinc, copper and lead, is concentrated primarily in the high sulfide tin-base metal deposits although its distribution is irregular. In the 256 samples analyzed for this study, the indium content ranges from 1 to 3690 ppm In; the median value is 58 ppm In. Indium correlates most closely with Zn and Cu, reflecting the fact that it is sequestered primarily in zinc and copper sulfides, particularly sphalerite and chalcopyrite, although some indium is present in less abundant minerals such as stannite and stannoidite. Zinc content in the samples ranges from 100 ppm to 35.7% Zn; the median value is 1.08% Zn. Copper values range from <100 ppm to 13.2% Cu; the median is 700 ppm. Indium correlates to a lesser extent with Sn, reflecting an association of cassiterite with indium-bearing sulfides rather than a high content of In in cassiterite. Tin content in the samples ranges from <100 ppm to 12.4% Sn; the median content is 1845 ppm. Tungsten content ranges from <100 to 1.9% W; the median value is 600 ppm W. There is no significant correlation of In with W, Mo, Bi or Pb.

Table 2
Correlation matrix for major and minor elements in tungsten–molybdenum and tin-base metal deposits at Mount Pleasant

	In	Sn	W	Mo	Bi	Cu	Pb
Sn	0.35						
W	0.11	0.01					
Mo	−0.22	−0.27	0.54				
Bi	0.04	0.26	0.19	0.18			
Cu	0.57	0.28	0.01	−0.16	0.15		
Pb	0.02	0.03	0.02	−0.08	0.05	0.03	
Zn	0.61	0.22	−0.09	−0.25	−0.01	0.30	0.17

6. Indium mineralogy of the tin-base metal deposits

In order to determine the distribution of indium in specific minerals, indium-rich samples from different indium-bearing zones were selected for detailed mineralogical and electron-microprobe analysis. Electron-microprobe analyses of minerals in polished thin sections were carried out at the Geological Survey of Canada on a Cameca Camebax electron-microprobe under running conditions of 25 kV and 25 nA, and a beam diameter of 2 to 5 μm. Counting times were generally 10 s except for indium, which was counted for 20 s when high levels of indium were encountered (generally >1% In), and for 30 s when low levels of indium were present (<1% In). Natural minerals, synthetic mineral equivalents and pure metals were used as standards. Data reduction was conducted according to the methods of Pouchou and Pichoir (1984). The detection limit of the electron-microprobe was about 0.01% In. Three replicate analyses of a synthetic sphalerite standard containing 0.119% In yielded values of 0.13%, 0.14% and 0.15% In, respectively.

Indium content of the principal indium-bearing minerals at Mount Pleasant is summarized in Table 3. Sphalerite is the most important host mineral for indium at Mount Pleasant and probably accounts for more than 90% of the indium present in the deposits; chalcopyrite contains most of the remainder. Stannite group minerals contain up to 1% In or more in places but these minerals occur only in minor amounts. The indium mineral roquesite contains as much as 47% In but is relatively rare. In addition to the minerals listed in Table 3, other minerals that contain detectable amounts of indium locally include arsenopyrite (up to 0.02% In), löllingite (up to 0.01% In) and wolframite (up to 0.03% In). Previously reported indium content of cassiterite in the range 0.1% to 0.2% In (Petruk, 1973; Sinclair et al., 1997) is problematic due to interference of Sn in electron-microprobe analyses of tin-rich minerals such as cassiterite. Indium content of cassiterite separates from Mount Pleasant, measured by neutron activation analysis, ranged from 38 to 90 ppm In (L. Raimbault, pers. comm., October 26, 2000).

6.1. Sphalerite

Sphalerite is the most abundant ore mineral in the indium-bearing tin-base metal deposits. It is mainly black in hand specimens, although light brown and

Table 3
Indium content (wt.% In) of minerals from Mount Pleasant

Mineral	No. of analyses	Minimum	Maximum	Average	Median
Chalcopyrite ($CuFeS_2$)	32	0.01	0.40	0.16	0.15
Cosalite ($Pb_2Bi_2S_5$)	7	<0.01	0.26	0.09	0.08
Galena (PbS)	7	<0.01	0.06	0.02	0.01
Pyrite (FeS_2)	10	<0.01	0.53	0.11	0.05
Pyrrhotite (FeS)	6	<0.01	0.03	0.01	0.01
Roquesite ($CuInS_2$)	5	45.82	46.97	46.46	46.50
Sphalerite ((Zn,Fe)(Cu,In)S)	126[a]	<0.01	6.90	1.23	0.52
Stannite ($Cu_2(Fe,Zn)SnS_4$)	20	0.07	2.21	0.64	0.63
Stannoidite ($Cu_8(Fe,Zn)_3Sn_2S_{12}$)	6	0.05	0.16	0.10	0.10
Tennantite ($(Cu,Fe,Zn)_{12}As_4S_{13}$)	13	0.01	0.06	0.03	0.03
Wittichenite (Cu_3BiS_3)	4	<0.01	0.10	0.03	0.02

[a] Does not include one anomalous analysis of 22.27% In.

yellow varieties occur locally. The black sphalerite typically contains abundant inclusions of a variety of minerals, the most common of which are chalcopyrite, stannite, këserite, ferrokësterite, galena, pyrite, and pyrrhotite. The inclusions range from minute blebs a few microns or less in size to small irregular grains 20 to 50 μm in size. In some sphalerite grains, irregular and widespread distribution of chalcopyrite and other inclusions (Fig. 10a) are characteristic of the so-called "chalcopyrite disease" described by Barton and Bethke (1987). In other grains, inclusions are distributed in concentric zones (Fig. 10b) that resemble replacement or DIS (diffusion induced segregations) textures that have been produced experimentally in sphalerite (Bente and Doering, 1993, 1995). Some included minerals occur as lamellae that appear to be aligned along crys-

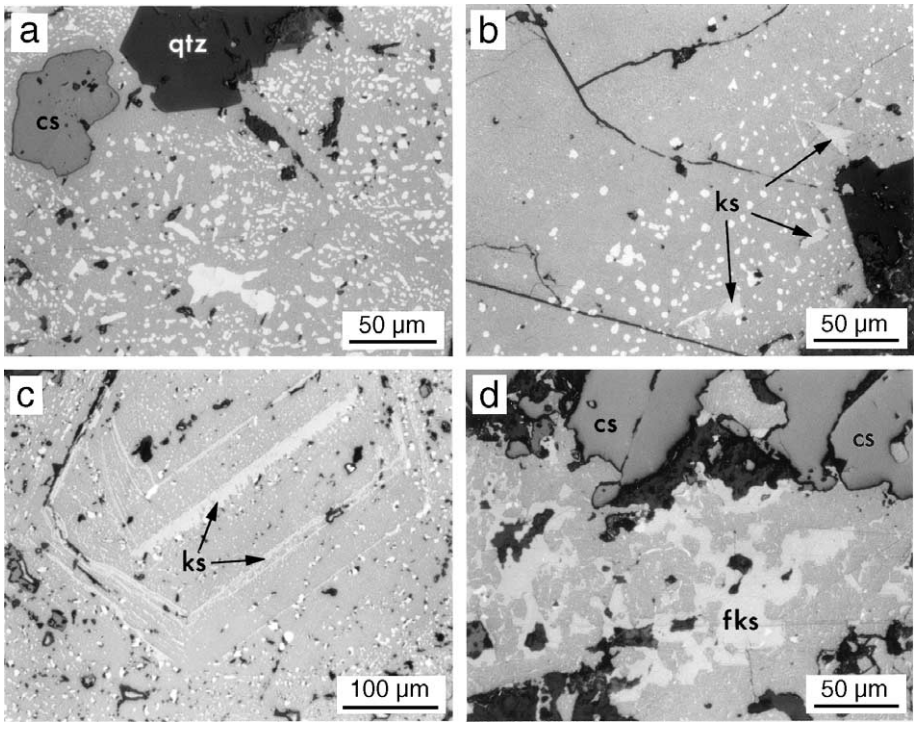

Fig. 10. Photomicrographs of polished sections. (a) Sphalerite (light grey) with abundant inclusions of chalcopyrite (white). Other minerals are cassiterite (cs) and quartz (qtz). GSC 1996-108P. (b) Inclusions of chalcopyrite (white) and këserite (ks) concentrated in a concentric zone near the edge of a sphalerite grain. GSC 1996-108T. (c) Këserite (ks) aligned along concentric crystal growth planes in the core of a sphalerite grain. Numerous inclusions of chalcopyrite and pyrrhotite (small white grains) are also present. GSC 1996-108C. (d) Irregular grains of ferrokësterite (fks) in sphalerite adjacent to grains of cassiterite (cs); small white grains in sphalerite and ferrokësterite are chalcopyrite. GSC 1996-108Q.

tallographic planes in the sphalerite (Fig. 10c); others have highly irregular shapes that may be due to exsolution or replacement (Fig. 10d).

Representative electron-microprobe analyses of sphalerite are listed in Table 4. Indium content of sphalerite in all analyzed samples varies mainly from about 0.1% to 6.9% In, although higher values ranging to more than 22% In were encountered in a few grains. Excluding such anomalously high analyses, the indium content of sphalerite averages 1.23% In and has a median value of 0.52% In. In previous studies, indium content of sphalerite from Mount Pleasant was found to range from about 0.03% to 3.0% In (Petruk, 1964, 1973; Boorman and Abbott, 1967; Sutherland and Halls, 1969).

The variation of indium and other major and minor elements in sphalerite determined by electron-microprobe analysis are shown as inter-element plots in Fig. 11. Indium concentration in sphalerite appears to correlate roughly with copper content but there is no evident correlation of indium with iron, zinc (not shown on Fig. 11) or minor elements such as tin, cadmium, bismuth or silver. Cadmium content of the sphalerite is relatively uniform, ranging mainly between 0.1% and 0.4% Cd, with a median value of 0.22% Cd. Tin content varies widely from less than 0.01% Sn to 5% Sn, with a median value of 0.05% Sn. Bismuth and silver contents range as high as 0.1% each but are below the detection limit of the electron-microprobe in most places.

High contents of copper, which ranged as high as 22.7% Cu, are problematic as sphalerite cannot contain more than 1.6% Cu in solid solution at low temperatures (Kojima and Sugaki, 1985). In most cases, high copper content was encountered in sphalerite grains that contained abundant inclusions of chalcopyrite and the anomalous copper analyses may be the result of edge effects near inclusions of chalcopyrite, which range from microscopic to submicroscopic in size. However, this would not account for the high levels of indium in sphalerite that are associated with high contents of copper.

The high levels of indium in sphalerite may reflect incipient exsolution of indium-rich minerals. A back-scattered electron image of indium-rich sphalerite (Fig.

Table 4
Representative electron-microprobe analyses of sphalerite and chalcopyrite from Mount Pleasant

Sample	3115X-37	5497-3-28	8381-8	10428D-1-5	14488-117	3158X-103	5452-58	5497-2-14
Mineral	Sphalerite	Sphalerite	Sphalerite	Sphalerite	Sphalerite	Chalcopyrite	Chalcopyrite	Chalcopyrite
wt.%								
Mn	0.00	0.06	0.06	0.00	0.00	0.00	0.02	0.02
Fe	8.58	10.30	11.64	0.26	5.78	30.02	29.71	29.77
Cu	3.99	3.38	0.40	0.71	6.77	34.58	34.24	34.15
Zn	52.36	47.71	53.40	64.58	52.27	0.07	0.35	0.92
Ag	0.01	0.05	0.05	0.05	0.05	0.14	0.00	0.06
Cd	0.20	0.22	0.21	0.15	0.31	0.00	0.03	0.03
In	2.14	5.59	0.37	0.88	1.79	0.07	0.21	0.40
Sn	0.05	0.06	0.08	0.05	0.04	0.17	0.16	0.09
Bi	0.06	0.05	0.12	0.00	0.02	0.00	0.06	0.00
As	0.06	0.10	0.08	0.03	0.15	0.07	0.16	0.06
Se	0.04	0.06	0.03	0.00	0.10	0.04	0.00	0.00
S	32.38	32.42	33.64	32.28	32.30	34.24	35.14	34.69
total	99.87	99.97	100.07	99.00	99.57	99.41	100.09	100.18
Atomic proportions (8 atoms)								
Mn	0.00	0.00	0.00	0.00	0.00	0.00	0.00	0.00
Fe	0.60	0.73	0.80	0.02	0.41	2.00	1.95	1.96
Cu	0.24	0.21	0.02	0.04	0.42	2.02	1.98	1.98
Zn	3.13	2.87	3.13	3.91	3.14	0.00	0.02	0.05
Ag	0.00	0.00	0.00	0.00	0.00	0.00	0.00	0.00
Cd	0.01	0.01	0.01	0.01	0.01	0.00	0.00	0.00
In	0.07	0.19	0.01	0.03	0.06	0.00	0.01	0.01
Sn	0.00	0.00	0.00	0.00	0.00	0.01	0.00	0.00
Bi	0.00	0.00	0.00	0.00	0.00	0.00	0.00	0.00
As	0.00	0.00	0.00	0.00	0.01	0.00	0.01	0.00
Se	0.00	0.00	0.00	0.00	0.00	0.00	0.00	0.00
S	3.94	3.98	4.02	3.99	3.95	3.96	4.02	3.99

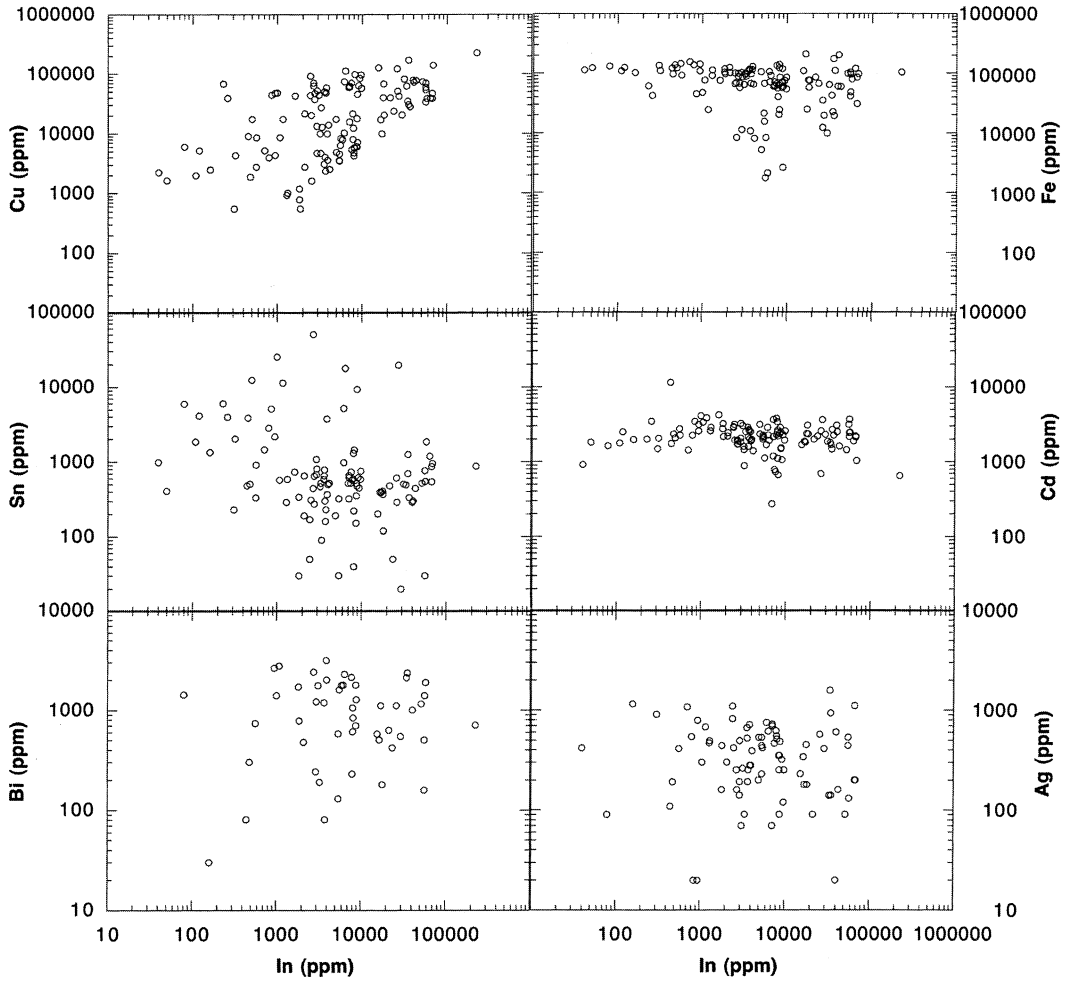

Fig. 11. Inter-element plots for major and minor elements in sphalerite from Mount Pleasant.

12) shows indium distributed irregularly throughout the sphalerite, which displays no optical evidence of compositional variation. Sutherland and Halls (1969) described an apparently similar inclusion-free sphalerite from Mount Pleasant that contained 14.0% In, along with 9.5% Cu and minor tin. This composition corresponds approximately to the unnamed Zn–In mineral reported by Ohta (1989) from the Toyoha deposit in Japan. On a ternary plot of Cu − (In + Sn) − (Zn + Fe) (Fig. 13), this composition is intermediate between sphalerite and roquesite, reflecting solid solution between these two minerals.

The backscattered electron image (Fig. 12) also shows high levels of indium around inclusions of chalcopyrite in particular. Concentration of indium in these areas is most likely the result of diffusion associated with the replacement of sphalerite by chalcopyrite. During this process, indium originally present in the sphalerite that could not be incorporated in chalcopyrite was apparently expelled and concentrated along a replacement front in adjacent sphalerite.

6.2. Chalcopyrite

Chalcopyrite is present in significant amounts in most of the tin-base metal deposits. It occurs as irregular masses up to several centimetres in size, commonly intergrown with sphalerite, and as minute grains and lamellae in sphalerite (Fig. 10a, b). Some larger masses of chalcopyrite contain inclusions of sphalerite, stannite, cassiterite, galena and other minerals. The indium content of chalcopyrite ranges from 0.01% In to 0.40% In, with an average value of 0.16% In and a median value of 0.15% In. Chalcopyrite grains in sphalerite have the highest indium content and also have high levels of zinc, ranging up to 1% Zn or more (Table 4). Although analyses of points within 5 to 10 μm of sphalerite have been discounted, the high contents of

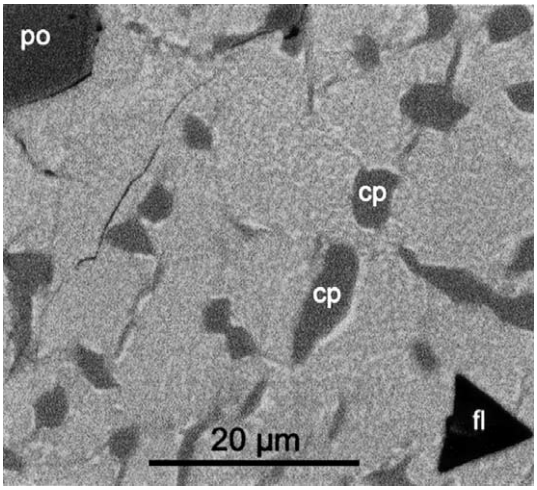

Fig. 12. Backscattered electron image of indium-bearing sphalerite. Indium-rich zones (white) are distributed irregularly throughout sphalerite (light grey) and at the margins of chalcopyrite inclusions (cp). Dark grey mineral at upper left is pyrrhotite (po); black mineral at lower right is fluorite (fl).

both indium and zinc in many chalcopyrite grains may have been influenced by proximity with the host sphalerite; the median value for all the chalcopyrite analyses is 0.20% Zn. Chalcopyrite also contains trace amounts of tin (median value of 0.1% Sn) and cadmium (median value of 0.03% Cd).

6.3. Stannite, kësterite and ferrokësterite

Minor amounts of stannite (Cu_2FeSnS_4) and other minerals of the stannite group, including kësterite ($Cu_2(Zn,Fe)SnS_4$), ferrokësterite ($Cu_2(Fe,Zn)SnS_4$), and petrukite ($(Cu,Fe,Zn)_3(Sn,In)S_4$), are present throughout the tin-base metal deposits. They occur most commonly as tiny inclusions in sphalerite and chalcopyrite, and as lamellae along growth planes in sphalerite (Fig. 10b–d). Although these minerals are generally very fine grained and not easily identified by their optical properties, they can be distinguished by their molecular proportions of Fe and Zn (Kissin and Owens, 1989; Alderton, 1991). In this study, the observed variation of Fe/(Fe+Zn) in stannite (possibly including petrukite) is between 0.72 and 0.93. Ferrokësterite has molecular ratios between 0.65 and 0.69 and kësterite between 0.53 and 0.56. The indium content of the stannite group minerals ranges from 0.07% to 2.21% In, but most analyses are between 0.1% and 1.0% In. The highest indium levels were recorded in stannite (2.21% In) and ferrokësterite (1.39% In). The average indium content is 0.64% In and the median is 0.63% In.

Representative electron-microprobe analyses of stannite group minerals are given in Table 5. On the ternary Cu – (Fe+Zn) – (In+Sn) diagram (Fig. 13), these and other analyses of stannite group minerals lie along the tie-line between stannite and sphalerite and, although a large gap exists, there appears to be a significant degree of solid solution between these two end-members. No significant solid solution between stannite group minerals and chalcopyrite or roquesite is evident.

6.4. Stannoidite

Stannoidite ($Cu_8(Fe,Zn)_3Sn_2S_{12}$) occurs locally in trace amounts, commonly associated with cassiterite either as microveinlets in cassiterite or as small irregular masses with inclusions of sphalerite, chalcopyrite, tennantite and roquesite. It also occurs intergrown with tennantite or as inclusions. The stannoidite appears to have a fairly uniform composition (Fig. 13), including relatively low indium content that averages 0.10% In.

6.5. Roquesite

Roquesite ($CuInS_2$) is a rare indium mineral that was first noted at Mount Pleasant by Sutherland and

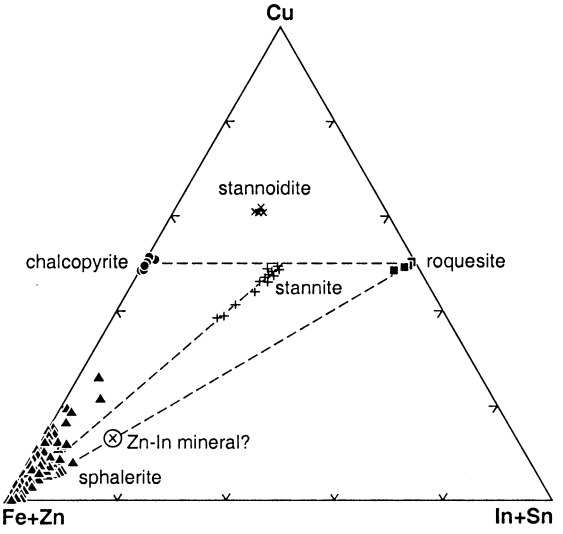

Fig. 13. Cu – (Fe+Zn) – (In+Sn) ternary plot of indium-bearing minerals from Mount Pleasant. Point X along the tie-line between sphalerite and roquesite represents sphalerite with 14.0% In and 9.5% Cu reported by Sutherland and Halls (1969), which corresponds approximately to Ohta's (1989) unnamed Zn–In mineral. Ohta (1989) attributed solid solution along the tie-line between sphalerite and roquesite to the coupled substitution CuIn↔2(Zn,Fe). The tie-line between sphalerite and stannite group minerals represents solid solution according to the coupled substitution Cu_2Sn↔2(Zn,Fe).

Table 5
Representative electron-microprobe analyses of stannite group minerals and roquesite from Mount Pleasant

Sample	14484-48	17361D-32	8381-10	14488-110	20437-25	14488-107	10482D-1-6	19039D-42
Mineral	Stannite	Stannite	Kësterite	Kësterite	Ferrokësterite	Ferrokësterite	Roquesite	Roquesite
wt.%								
Mn	0.03	0.00	0.01	0.00	0.00	0.01	0.00	0.01
Fe	12.38	10.33	12.46	8.36	11.10	9.95	0.14	0.57
Cu	29.07	28.36	23.89	27.55	26.45	27.56	26.41	26.49
Zn	2.40	4.80	11.41	7.93	7.08	6.36	1.23	0.34
Ag	0.10	0.02	0.06	0.07	0.03	0.11	0.00	0.00
Cd	0.00	0.07	0.10	0.05	0.00	0.08	0.09	0.05
In	0.14	0.99	0.72	0.60	0.98	0.39	46.48	46.53
Sn	26.22	25.85	21.45	26.59	24.66	25.69	0.09	0.20
Bi	0.24	0.00	0.10	0.25	0.08	0.09	0.19	0.06
As	0.06	0.00	0.14	0.05	0.02	0.11	0.00	0.00
Se	0.32	0.26	0.23	0.21	0.21	0.16	0.02	0.14
S	29.71	29.16	30.82	29.17	29.91	29.36	26.26	26.48
total	100.68	99.83	101.39	100.82	100.52	99.87	100.91	100.86
Atomic proportions (8 atoms)								
Mn	0.00	0.00	0.00	0.00	0.00	0.00	0.00	0.00
Fe	0.95	0.80	0.93	0.65	0.85	0.77	0.01	0.05
Cu	1.95	1.94	1.56	1.88	1.77	1.87	2.00	2.00
Zn	0.16	0.32	0.72	0.52	0.46	0.42	0.09	0.02
Ag	0.00	0.00	0.00	0.00	0.00	0.00	0.00	0.00
Cd	0.00	0.00	0.00	0.00	0.00	0.00	0.00	0.00
In	0.01	0.04	0.03	0.02	0.04	0.01	1.95	1.94
Sn	0.94	0.94	0.75	0.97	0.89	0.94	0.00	0.01
Bi	0.00	0.00	0.00	0.00	0.00	0.00	0.00	0.00
As	0.00	0.00	0.01	0.00	0.00	0.01	0.00	0.00
Se	0.02	0.01	0.01	0.01	0.01	0.01	0.00	0.01
S	3.96	3.94	3.99	3.94	3.98	3.96	3.94	3.96

Boorman (1969). Petruk (1973) observed that roquesite grains occur haphazardly throughout sphalerite together with inclusions of stannite, chalcopyrite and/or këesterite. Roquesite observed in this study occurs as minute grains (<20 μm) either included in or closely associated with stannoidite. The composition of roquesite is relatively restricted (representative analyses are given in Table 5), although analyses fall on the tie-line with sphalerite and the unnamed Zn–In mineral (Fig. 13) indicating a limited degree of solid solution. No significant solid solution with stannite group minerals is apparent.

6.6. Galena, cosalite and wittichenite

The indium content of copper–lead–bismuth minerals, including galena, cosalite ($Pb_2Bi_2S_5$) and wittichenite (Cu_3BiS_3), is relatively low. Galena is present in moderate amounts in the tin-base metal deposits as small irregular masses intergrown with sphalerite and containing inclusions of cosalite and other bismuth minerals. It also occurs as inclusions in chalcopyrite. Indium content of galena ranges from <0.01% to 0.06% In; the median value is 0.01% In.

Cosalite occurs in trace amounts, typically as inclusions in, or intergrown with, galena. One grain contained 0.26% In, but most analyses yielded less than 0.1% In. The median content of indium in cosalite is 0.08% In. Only a few minute grains of wittichenite associated with bismuth and bismuthinite were encountered in this study. They contain up to 0.10% In; the median is 0.02% In.

6.7. Tennantite

Tennantite ($(Cu,Fe,Zn)_{12}As_4S_{13}$) is locally abundant as irregular, disseminated grains, commonly intergrown with sphalerite, arsenopyrite and, in places, stannoidite. It contains only traces of antimony (0.03% to 0.27% Sb) and thus is close to end-member tennantite in composition. The indium content is low, ranging from <0.01% to 0.06% In. The average and median contents of indium are similar (0.03% In).

6.8. Pyrite and pyrrhotite

Pyrite occurs in minor amounts in veinlets, as disseminated grains, and as inclusions in sphalerite and chalcopyrite. The indium content of pyrite varies from below detection to slightly more than 0.5% In. The average indium content of pyrite is 0.11% In; the median is 0.05% In.

Most of the pyrrhotite grains analyzed occur as small inclusions in sphalerite (e.g., Fig. 10c) and appear to contain 1% to 5% Zn, probably due to edge effects of the surrounding sphalerite. Not including grains that contain high zinc (>2% Zn), indium content of pyrrhotite ranges from below detection to a maximum of 0.03% In; average and median contents are similar at 0.01% In.

7. Temperature estimates based on the sphalerite–stannite geothermometer

Nekrasov et al. (1979) and Nakamura and Shima (1982) proposed different equations for equilibrium temperatures of coexisting sphalerite and stannite based on experimentally observed partitioning of iron and zinc between these minerals. Using these equations, temperatures of equilibration have been calculated for coexisting sphalerite and stannite group minerals in the tin-base metal deposits at Mount Pleasant (Table 6). The results are based on spot analyses of adjacent grains and do not take into account compositional variations in the grains, which could be significant. For example, the effects of indium, which ranges up to nearly 1% In in the sphalerite analyses used in the calculations, are unknown. Also, textural relationships do not unequivocally rule out the possibility of disequilibrium between the mineral pairs, although obvious examples of replacement or DIS-type phenomena were not included in the results.

The temperatures calculated according to the equation of Nakamura and Shima (1982), which are considered by some to be more reliable (e.g., Shimizu and Shikazono, 1985; Brill, 1989; Corsini et al., 1991), range from 305 to 387 °C. Temperatures based on Nekrasov et al. (1979) range more widely from 232 to 391 °C. In comparison, homogenization temperatures of fluid inclusions in quartz and fluorite that are associated with, but paragenetically younger than, the sphalerite and stannite group minerals display an even broader range from approximately 150 to 350 °C (Samson, 1990). Uncertainties in the application of the sphalerite–stannite geothermometer notwithstanding, the data suggest that temperatures of formation of the indium-bearing tin-base metal deposits may have been initially as high as 400 °C, but waned or fluctuated to less than 200 °C during deposition of the sulfide and associated gangue minerals.

8. Discussion

Ohta (1995) summarized the characteristic features of Bolivian and Japanese tin-polymetallic deposits, many of which also apply to the indium-bearing tin-base metal deposits at Mount Pleasant. These include 1) the presence of low fS_2 minerals (cassiterite, wolfram-

Table 6
Chemical composition and temperatures of formation of coexisting sphalerite and stannite group minerals from Mount Pleasant

Sample-pt	Mineral	Comment	Fe (wt.%)	Zn (wt.%)	Fe/Zn	Kd	log Kd	T °C (1)	T °C (2)
8381U-9	Sphalerite	Kësterite aligned along crystal growth	10.44	53.09	0.20	0.18	−0.74	391	387
8381U-10	Kësterite	Plane in core of sphalerite grain (Fig. 10c)	12.46	11.41	1.09				
14484-83	Sphalerite	Ferrokësterite lamella in sphalerite	11.64	53.48	0.22	0.16	−0.80	373	378
14484-81	Ferrokësterite		12.20	8.91	1.37				
14485-61	Sphalerite	Stannite grain in sphalerite	9.93	45.49	0.22	0.08	−1.10	288	336
14485-62	Stannite		12.67	4.65	2.73				
14488-108	Sphalerite	Irregular exsolution of ferrokësterite	9.13	43.78	0.21	0.13	−0.87	349	367
14488-107	Ferrokësterite	In sphalerite (Fig. 10d)	9.95	6.36	1.56				
14488-115	Sphalerite	Ferrokësterite lamella in sphalerite	4.23	58.07	0.07	0.05	−1.35	233	305
14488-116	Ferrokësterite		9.61	5.96	1.61				
17361D-31	Sphalerite	Stannite grain in sphalerite	5.44	56.36	0.10	0.04	−1.35	232	305
17361D-32	Stannite		10.33	4.80	2.15				
20437D-26	Sphalerite	Ferrokësterite grain in sphalerite	7.05	57.87	0.12	0.08	−1.11	285	334
20437D-25	Ferrokësterite		11.10	7.08	1.57				

T °C (1): Geothermometer from Nekrasov et al. (1979).
T °C (2): Geothermometer from Nakamura and Shima (1982).

ite, arsenopyrite, löllingite and pyrrhotite) as well as an intermediate to high fS_2 assemblage (sphalerite+chalcopyrite+stannite); 2) association with Fe-rich chlorite and F-rich alteration minerals such as topaz, fluorite and sericite; 3) late-stage acid alteration consisting of kaolin and Fe-carbonate; 4) the presence of significant rare metals such as In, Sn, W, and Bi; and 5) maximum formation temperatures in excess of 350 °C. Like the Mount Pleasant tin-base metal deposits, tin-polymetallic veins of Bolivia and Japan also typically occur in veins and breccias in shallow volcanic environments and are related to subjacent granitic plutons. Some differences are evident; in particular, the silver content of the Mount Pleasant deposits is negligible compared to Bolivian and Japanese deposits and silver minerals are not abundant.

The indium content of the Mount Pleasant tin-base metal deposits is higher than for most tin-polymetallic deposits, one exception being the Toyoha deposit where the average grade of the ore is 140 g/t In (Kooiman and Ruitenberg, 1992) and individual veins locally contain more than 1000 g/t In (Kanbara et al., 1989). At Toyoha, as at Mount Pleasant, sphalerite is an important indium-bearing mineral, containing more than 10 wt.% In in places (Ohta, 1989). Commonly associated with the indium-bearing sphalerite at Toyoha is an unnamed Zn–In mineral that forms a continuous solid solution with sphalerite. Ohta (1989) attributed this solid solution to coupled substitution of 2(Zn,Fe) for CuIn. The unnamed Zn–In mineral is tentatively recognized at Mount Pleasant and the composition of Mount Pleasant sphalerite is consistent with the same coupled substitution. The indium-rich zones indicated by scanning electron microscopy (Fig. 12) may be evidence of the Zn–In mineral, but more study is required to confirm this and to clarify the nature of indium distribution in sphalerite at Mount Pleasant.

Indium at Mount Pleasant is associated with one of two distinct episodes of mineralization that are distinguished by differences in composition, structural styles of mineralization and associated granitic rocks. The first episode, represented by porphyry tungsten–molybdenum deposits that consist of breccia zones and fracture stockworks extending over areas hundreds of metres across, is characterized by relatively low sulfide content (generally less than 1% by volume). Granitic rocks associated with these deposits, fine-grained granite in the Fire Tower Zone and granite I in the North Zone, represent the earliest period of intrusion at Mount Pleasant. Tin-base metal deposits, in which indium is concentrated, constitute the second episode of mineralization. These deposits typically consist of moderately to heavily disseminated sulfides in veins, breccias and replacement zones that range from less than one metre to several tens of metres wide. They are associated with intrusions of granite porphyry in the Fire Tower Zone and granite II in the North Zone, which crosscut and clearly postdate the first episode of mineralization.

The change in the dominant structural style of mineralization from extensive fracture and breccia zones to more restricted veins and replacement zones likely reflects decreased volatile pressures that accompanied degassing of the associated granitic magmas. At depths of 1 to 2 km, the level of emplacement of the granitic magma at Mount Pleasant (Sinclair et al., 1988), resurgent boiling, can produce overpressures that easily exceed tensile strength of the crystallized carapace of the melt and surrounding country rock (Burnham, 1979). The resulting brittle failure can be explosive. Textural features of the fine-grained granite associated with porphyry-type mineralization in the Fire Tower Zone include locally abundant micrographic intergrowths of quartz and feldspar, a feature that is characteristic of quenching in undercooled granitic melts (Walker, 1976; Fenn, 1979). Such textural features and the extensive brecciation within and surrounding the fine-grained granite are evidence that ore-forming fluids were expelled rapidly under explosive conditions (Kooiman et al., 1986). The granitic rocks associated with the tin-base metal deposits are characterized by comb-layered quartz, a feature that records the passage of ore-forming fluids exsolved from subjacent magma (Kirkham and Sinclair, 1988; Lowenstern and Sinclair, 1996). However, in contrast to the porphyry episode of mineralization, the limited fracturing and brecciation associated with the tin-base metal mineralization suggest that development of excess fluid pressures occurred only locally in the related magmas. This likely reflects an overall decrease in the volatile content of the parent magma subsequent to the episode of porphyry mineralization.

The differences in composition of the related deposits also reflect changes in the ore-forming fluids related to the two episodes of mineralization. Although significant amounts of tungsten, molybdenum and bismuth are present in the tin-base metal deposits at Mount Pleasant, only trace amounts of tin, zinc, lead, copper and indium occur in the porphyry tungsten–molybdenum–bismuth deposits, except where they are overprinted by tin-base metal mineralization. This suggests that the tin and base metals were sequestered in the melt during the porphyry mineralization and did not partition into coexisting fluid phases

until the later episode of tin-base metal mineralization. This pattern of early oxide-bearing assemblages and later sulfide-rich assemblages has also been recognized in Bolivian tin-polymetallic deposits (e.g., Turneaure, 1971; Sugaki and Kitakaze, 1988). The reasons for it are not clear but may include decreasing temperature, reduction of the magmas as a consequence of degassing, and melt fractionation. In any case, a profound change in the composition of the ore-forming fluids occurred during the hiatus between the two episodes of mineralization.

The variety of textures and mineral assemblages of the indium-bearing tin-base metal deposits likely reflect multiple pulses of mineralization, some of which were more indium-rich than others. Indium-rich sphalerite deposited at high temperatures may have become metastable at lower temperatures, resulting in the incipient exsolution of indium minerals suggested by scanning electron microscopy (Fig. 12). However, such sphalerite typically contains a variety of inclusions, particularly chalcopyrite, stannite, pyrite and pyrrhotite, the presence of which cannot be explained solely by exsolution or unmixing. For instance, the maximum experimentally observed solubility of CuS in sphalerite at temperatures up to 500 °C is 2.4 mol% (Kojima and Sugaki, 1985) and is too low to account for the chalcopyrite content of many sphalerite grains. Although some unmixing may have occurred, other mechanisms such as replacement related to later pulses of copper-rich mineralization are required to account for the observed textures. The correlation of indium with copper (Figs. 9 and 11) and its particular association with chalcopyrite (Fig. 12) suggest that much of the indium was introduced during these copper-rich pulses of mineralization.

Deposition of the Mount Pleasant tin-base metal deposits likely occurred mainly in response to interaction of magmatic–hydrothermal ore-bearing fluids and local ground water. Oxygen and hydrogen isotope data indicate that mixtures of magmatic and meteoric waters were responsible for the greisen alteration associated with the deposits (Seltmann et al., 1997). Low-salinity fluid inclusions in fluorite and quartz associated with the tin-base metal deposits also reflect significant input of meteoric water (Samson, 1990). Mixing would have cooled and diluted the hot magmatic fluids as they came in contact with cooler meteoric water, resulting in deposition of the ore minerals. Such mixing is consistent with the temperatures of ore deposition, which

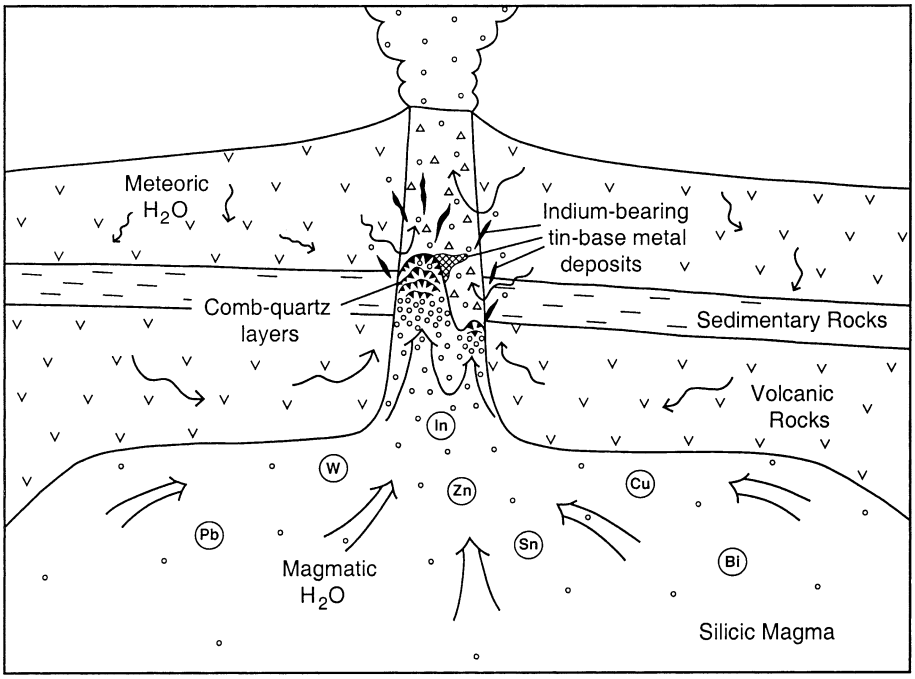

Fig. 14. Schematic diagram illustrating the formation of the Mount Pleasant indium-bearing tin-base metal deposits in a volcanic vent complex intruded by silicic magmatic rocks. Large open arrows indicate concentration and degassing of magmatic–hydrothermal fluid and metals from a large body of convecting silicic magma through a small subvolcanic cupola at the top of the magma body. Development of comb quartz layers in the cupola reflects the continuous supply of exsolved magmatic fluid. Meteoric water (indicated by small arrows) interacted with magmatic fluid as it escaped from the cupola, resulting in the deposition of the indium and other metals in veins and replacement bodies in vent breccias and surrounding volcanic and sedimentary country rocks.

ranged from a maximum of about 400 °C to a minimum below 200 °C. Similar depositional conditions have been suggested for other tin-polymetallic deposits, e.g., Toyoha (Ohta, 1995).

Our model for the formation of the indium-bearing tin-base metal deposits at Mount Pleasant is summarized graphically in Fig. 14, which shows the deposits related to small intrusions or cupolas of granitic magma intruded into a volcanic vent–breccia complex. The presence of abundant comb quartz layers indicates that these cupolas acted as conduits for substantial volumes of magmatic–hydrothermal fluids derived from a large subjacent body of convecting magma (cf. Shinohara et al., 1995). Elements such as indium, tin, tungsten and base metals, incompatible with magmatic crystallization, were concentrated in these fluids. The ore-bearing fluids escaped from the cupolas into faults, fractures and breccia zones in the volcanic vent and surrounding country rocks. Cooling of the fluids as they expanded into these dilatent structures and mixed with meteoric water resulted in the deposition of indium and other metals in sulphide-rich veins, breccias and replacement bodies.

9. Conclusions

1) Sphalerite is the most important mineral for indium at Mount Pleasant; chalcopyrite is the second most important. Indium is also present in stannite group minerals and rare grains of roquesite.
2) Indium content is highest in sphalerite characterized by high copper contents and abundant inclusions of chalcopyrite. Although some indium may have been incorporated into sphalerite at the time of initial sphalerite deposition, much of the indium was introduced during later pulses of copper-rich mineralization that resulted in partial replacement of sphalerite by chalcopyrite.
3) Indium-bearing sphalerite occurs in sulfide-rich assemblages associated with a specific phase of granitic intrusion at Mount Pleasant (granite IIB in the North Zone, granite porphyry in the Fire Tower Zone). This phase of granite formed cupolas characterized by abundant comb quartz layers, a type of unidirectional solidification texture (UST) that reflects the former presence of exsolved magmatic–hydrothermal fluid. The cupolas represent conduits for the degassing of this fluid and ore elements, including indium, from a larger underlying body of magma.
4) Deposition of the indium-bearing sulfide assemblages occurred in response to cooling and dilution of the magmatic ore-bearing fluid as a result of mixing with meteoric water. Temperatures of deposition ranged from 400 to 200 °C or less.

Acknowledgments

Piskahegan Resources Ltd and Adex Mining Corporation encouraged this study, provided support and gave permission to publish the results. Gilles LaFlamme from the Canada Centre for Mineral and Energy Technology (CANMET) provided the synthetic sphalerite used as a standard in electron-microprobe analyses. Processing of the electron-microprobe data was done with the assistance of John Stirling and Gordon Pringle of the Geological Survey of Canada (GSC). Louis Raimbault (École des Mines, Fontainebleau) provided neutron activation analyses of indium in cassiterite from Mount Pleasant and Thomas Doering (Leipzig University) provided additional electron-microprobe analyses of indium in sphalerite. Constructive reviews of this paper by Ian Jonasson (GSC), Steve McCutcheon (New Brunswick Department of Natural Resources and Energy), Eijun Ohta (Geological Survey of Japan) and Ulrich Schwartz-Schampera (Freiberg University of Mining and Technology) resulted in many improvements and are much appreciated.

References

Alderton, D.H.M., 1991. Stannite revisited. Journal of the Russell Society 4, 17–23.

Barton Jr., P.B., Bethke, P.M., 1987. Chalcopyrite disease in sphalerite: pathology and epidemiology. American Mineralogist 72, 451–467.

Bente, K., Doering, T., 1993. Solid-state diffusion in sphalerites: an experimental verification of the “chalcopyrite disease”. European Journal of Mineralogy 5, 465–478.

Bente, K., Doering, T., 1995. Experimental studies on the solid state diffusion of Cu+In in ZnS and on “Disease”, DIS (Diffusion Induced Segregations), in sphalerite and their geological applications. Mineralogy and Petrology 53, 285–305.

Boorman, R.S., Abbott, D., 1967. Indium in co-existing minerals from the Mount Pleasant tin deposit. Canadian Mineralogist 9, 166–179.

Brill, B.A., 1989. Trace element contents and partitioning of elements in ore minerals from the CSA Cu–Pb–Zn deposit, Australia. Canadian Mineralogist 27, 263–274.

Burnham, C.W., 1979. Magmas and hydrothermal fluids. In: Barnes, H.L. (Ed.), Geochemistry of Hydrothermal Ore Deposits, 2nd edition. John Wiley and Sons, New York, pp. 71–136.

Corsini, F., Morelli, F., Tanelli, G., 1991. A polymetallic sulfide (Cu–Pb–Zn) assemblage from the Boccheggiano–Campiano (Tuscany) pyrite deposit: application of the stannite–sphalerite geothermometer. Neues Jahrbuch für Mineralogie, 523–528.

Fenn, P.M., 1979. On the origin of graphic intergrowths. Geological Society of America, Abstracts with Programs 11, 424.

Halsall, P., 1988. Indium — extraction from lead, zinc and tin circuits. Transactions, Institution of Mining and Metallurgy 97, C93–C99.

Hannington, M.D., Bleeker, W., Kjarsgaard, I., 1999. Sulfide mineralogy, geochemistry, and ore genesis of the Kidd Creek deposit: part I. North, central and south orebodies. In: Hannington, M.D., Barrie, C.T. (Eds.), The Giant Kidd Creek Volcanogenic Massive Sulfide Deposit, Western Abitibi Subprovince, Canada, Economic Geology Monograph, vol. 10, pp. 163–223.

Hosking, K.F.G., 1963. Geology, mineralogy and paragenesis of the Mount Pleasant tin deposits. Canadian Mining Journal 84, 95–102.

Hunt, P.A., Roddick, J.C., 1990. A compilation of K–Ar ages, report 20. Radiogenic Age and Isotopic Studies: Report 3, Geological Survey of Canada, Paper, vol. 89-2, pp. 153–190.

Inverno, C.M.C., 1991. Endogranitic tin mineralization in Mount Pleasant intrusive complex, New Brunswick, Canada. Unpublished Ph.D. thesis, Colorado School of Mines, 302 pp.

Kanbara, H., Sanga, T., Ohura, T., Kumita, K., 1989. Mineralization of Shinano vein in the Toyoha polymetallic vein-type deposits, Hokkaido, Japan. Mining Geology 39, 107–122 (in Japanese with English abstract).

Kirkham, R.V., Sinclair, W.D., 1988. Comb quartz layers in felsic intrusions and their relationship to porphyry deposits. In: Taylor, R.P., Strong, D.F. (Eds.), Recent Advances in the Geology of Granite-Related Mineral Deposits, The Canadian Institute of Mining and Metallurgy, Special Volume, vol. 39, pp. 50–71.

Kissin, S.A., 1989. A reinvestigation of the stannite (Cu_2FeSnS_4)–kësterite (Cu_2ZnSnS_4) pseudobinary system. Canadian Mineralogist 27, 689–697.

Kissin, S.A., Owens, D.R., 1989. The relatives of stannite in the light of new data. Canadian Mineralogist 27, 673–688.

Kojima, S., Sugaki, A., 1985. Phase relations in the Cu–Fe–Zn–S system between 500 °C and 300 °C under hydrothermal conditions. Economic Geology 80, 158–171.

Kooiman, G.J.A., Ruitenberg, A.A., 1992. Indium deposits and their economic potential: report on a mission to Japan. New Brunswick Department of Natural Resources and Energy, Geoscience Report 92-3 (62 pp.).

Kooiman, G.J.A., McLeod, M.J., Sinclair, W.D., 1986. Porphyry tungsten–molybdenum orebodies, polymetallic veins and replacement bodies, and tin-bearing greisen zones in the Fire Tower Zone, Mount Pleasant, New Brunswick. Economic Geology 81, 1356–1373.

Lowenstern, J.B., Sinclair, W.D., 1996. Exsolved magmatic fluid and its role in the formation of comb-layered quartz at the Cretaceous Logtung W–Mo deposit, Yukon Territory, Canada. Transactions of the Royal Society of Edinburgh, Earth Sciences 87, 291–303.

McCutcheon, W., 1996. Specialty nonferrous metals — indium. In: Godin, E. (Ed.), Canadian Minerals Yearbook 1995 — Review and Outlook, Minerals and Metals Sector. Natural Resources Canada, Ottawa, pp. 55.20–55.22.

McCutcheon, S.R., Anderson, H.E., Robinson, P.T., 1997. Stratigraphy and eruptive history of the Late Devonian Mount Pleasant Caldera Complex, Canadian Appalachians. Geological Magazine 134, 17–36.

McLeod, M.J., Johnson, S.C., Ruitenberg, A.A., 1994. Geological Map of Southwestern New Brunswick. New Brunswick Department of Natural Resources and Energy, Map NR-5.

Murao, S., Furuno, M., Uchida, A.C., 1991. Geology of indium deposits; a review. Mining Geology 41, 1–13.

Nakamura, Y., Shima, H., 1982. Fe and Zn partitioning between stannite and sphalerite (in Japanese). Abstracts of the Joint Meeting of the Society of Mining Geologists of Japan, the Mineralogical Society of Japan and the Japanese Association of Mineralogists, Petrologists and Economic Geologists, A-8.

Nekrasov, I.J., Sorokin, V.I., Osadchii, E.G., 1979. Fe and Zn partitioning between coexisting stannite and sphalerite and its application in geothermometry. In: Ahrens, L.H. (Ed.), Origin and Distribution of the Elements. Pergamon Press, pp. 739–742.

Ohta, E., 1989. Occurrence and chemistry of indium-containing minerals from the Toyoha Mine, Hokkaido, Japan. Mining Geology 39, 355–372.

Ohta, E., 1995. Common features and genesis of tin-polymetallic veins. Resource Geology, Special Issue 18, 187–195.

Parrish, I.S., Tully, J.V., 1978. Porphyry tungsten zones at Mount Pleasant, N.B. Canadian Institute of Mining and Metallurgy Bulletin 71, 121–126.

Petruk, W., 1964. Mineralogy of the Mount Pleasant tin deposit in New Brunswick. Canadian Mines Branch Technical Bulletin TB 56 (37 pp.).

Petruk, W., 1973. The tungsten–bismuth–molybdenum deposit of Brunswick Tin Mines Limited: its mode of occurrence, mineralogy and amenability to mineral beneficiation. Canadian Institute of Mining and Metallurgy Bulletin 66, 113–130.

Pichavant, M., Manning, D.A.C., 1984. Petrogenesis of tourmaline and topaz granites: the contribution of experimental data. Physics of Earth and Planetary Interiors 35, 31–50.

Pouchou, J.L., Pichoir, F., 1984. A new model for quantitative X-ray microanalysis: Part I. Application to the analysis of homogeneous samples. Recherche Aérospatiale 1984-3, 13–38.

Roskill, 1996. The Economics of Indium. Roskill Information Services Ltd. 111 pp.

Ruitenberg, A.A., 1963. Tin mineralization and associated rock alteration at Mount Pleasant, Charlotte County, New Brunswick. Unpublished M.Sc. thesis, University of New Brunswick, 172 pp.

Ruitenberg, A.A., 1967. Stratigraphy, structure and metallization, Piskahegan-Rolling Dam area (northern Appalachians, New Brunswick, Canada). Leidse Geologische Mededelingen 40, 79–120.

Samson, I.M., 1990. Fluid evolution and mineralization in a subvolcanic granite stock: the Mount Pleasant W–Mo–Sn deposits, New Brunswick, Canada. Economic Geology 85, 145–163.

Schwartz-Schampera, U., Herzig, P.M., 1999. Indium geology, mineralogy, and economics — a review. Bundesanstalt für Geowissenschaften und Rohstoffe, Berichte zur Lagerstätten-und Rohstofforschung 35 (182 pp.).

Schwartz-Schampera, U., Herzig, P.M., 1999. Indium: geology, mineralogy, and economics — a review. Zeitschrift für Angewandt Geologie 45, 164–169.

Seltmann, R., Sinclair, W.D., Taylor, B.E., Uher, P., 1997. Fluid–rock reactions at the Sn–In–Zn–Pb–Cu deposits of Mount Pleasant, Canada. In: Papunen, H. (Ed.), Mineral Deposits: Research and Exploration, Where do They Meet? A.A. Balkema, Rotterdam, pp. 671–674.

Shannon, J.R., Walker, B.M., Carten, R.D., Geraghty, E.P., 1982. Unidirectional solidification textures and their significance in determining relative ages of intrusions at the Henderson mine, Colorado. Geology 10, 293–297.

Shimizu, M., Shikazono, N., 1985. Iron and zinc partitioning between coexisting stannite and sphalerite: a possible indicator of temperature and sulfur fugacity. Mineralium Deposita 20, 314–320.

Shinohara, H., Kazahaya, K., Lowenstern, J.B., 1995. Volatile transport in a convecting magma column: implications for porphyry Mo mineralization. Geology 23, 1091–1094.

Sinclair, W.D., 1994. Tungsten–molybdenum and tin deposits at Mount Pleasant, New Brunswick, Canada: products of ore–fluid evolution in a highly fractionated granitic system. In: Seltmann, R., Kämpf, H., Möller, R. (Eds.), Metallogeny of Collisional Orogens. Czech Geological Survey, Prague, pp. 410–417.

Sinclair, W.D., Kooiman, G.J.A., Martin, D.A., 1988. Geological setting of granites and related tin deposits in the North Zone, Mount Pleasant, New Brunswick. Geological Survey of Canada, Current Research, Paper 88-1B, 201–208.

Sinclair, W.D., Kjarsgaard, I.M., Kooiman, G.J.A., 1997. Indium distribution in tin-base metal zones at Mount Pleasant, New Brunswick. Geological Association of Canada/Mineralogical Association of Canada, Abstract Volume 22, A137–A138.

Stevens, L.G., White, C.E.T., 1990. Indium and bismuth. Metals Handbook, 10th ed., v. 2. ASM International, pp. 750–757.

Sugaki, A., Kitakaze, A., 1988. Tin-bearing minerals from Bolivian polymetallic deposits and their mineralization stages. Mining Geology 38, 419–435.

Sutherland, J.K., Boorman, R.S., 1969. A new occurrence of roquesite at Mount Pleasant, New Brunswick. American Mineralogist 54, 1202–1203.

Sutherland, J.K., Halls, C., 1969. Composition of some New Brunswick sphalerites. New Brunswick Research and Productivity Council, Research Note 21 (16 pp.).

Turneaure, F.S., 1971. The Bolivian tin–silver province. Economic Geology 66, 215–225.

Walker, B.M., 1976. The origin of quartz–feldspar, graphic intergrowths. Unpublished Ph.D. thesis, Michigan State University, 65 pp.